3027

[redacted]

NRL Report 4958

Copy No. [redacted]

AN EXPERIMENTAL 220-MC RADAR SYSTEM FOR AIRSHIPS

[redacted] TITLE-UNCLASSIFIED

R. L. Eilbert, A. M. Knopp, T. S. Golden,
P. A. Lantz, A. G. Ferris, and G. W. Hermann

Search Radar Branch
Radar Division

September 11, 1957

[redacted]

NOT RELEASABLE TO FOREIGN NATIONALS

NAVAL RESEARCH LABORATORY
Washington, D.C.

[redacted]

CONTENTS

ABSTRACT

[redacted] UNCLASSIFIED

The Naval Research Laboratory has designed and constructed an experimental 220-Mc radar for installation in a modified ZPG-2W airship. Important features of this system include a large internally mounted antenna, a high-power triode oscillator, a lobe-counting height finder, and a clutter-gated noncoherent MTI.

The transmitter, tunable from 216 to 225 Mc, is a 3W10,000A3 triode oscillator in a so-called grid-bell circuit. Nominal pulse-power output is 750 kw with a 5-μsec pulse at a duty cycle of 0.015.

Two antennas designed and built for the system are a 17-1/2 x 4 foot antenna which was used in preliminary system tests, and a 33-1/2 x 9 foot antenna which is being mounted in the gas enclosure of the airship. Both antennas are two-dimensional dipole arrays. The computed gain of the smaller antenna is 16 db with a horizontal half-power beamwidth of 18.4 degrees. The larger antenna has a computed gain of 22 db and a horizontal beamwidth of 8.9 degrees.

The height-finding equipment consists of a range-gated tracker and a Brush two-channel recorder which measure the number of lobes per mile traversed by the target, and a special slide rule which facilitates the computation of target height.

The MTI is of a noncoherent type, employing a clutter gate which enables the system to switch automatically from MTI to normal operation in the absence of clutter. Subclutter visibility is expected to be about 24 db for the complete MTI radar.

Radar performance tests were conducted at the Chesapeake Bay Annex of the Naval Research Laboratory with the small antenna at a height of 113.5 feet above sea level. An FJ-3 and an F9F-8 were detected at 205 nautical miles at 40,000 feet and 30,000 feet respectively. An F4D was detected at 225 nautical miles at 40,000 feet.

The Goodyear Aircraft Corporation is currently installing the radar with the large antenna on a ZPG-2W airship. Flight-testing of this vehicle will begin about June 1, 1957. Following Navy acceptance the airship will be based at the Naval Air Development Unit, South Weymouth, Massachusetts, where a series of measurements will be conducted to determine the range performance, height-finding capabilities, and sea-clutter characteristics.

PROBLEM STATUS

This is an interim report; work is continuing.

AUTHORIZATION

NRL Problem R02-10
Projects NR 412-000 and NR 412-008
Bureau No. NRL-EL-43010
BuAer NL 413012

Manuscript submitted May 20, 1957

AN EXPERIMENTAL 220-Mc RADAR SET FOR AIRSHIPS

[Confidential Title] (U)

INTRODUCTION

This report describes the experimental 220-Mc radar system which has been installed in a ZPG-2W airship under Bureau of Aeronautics problem NRL-EL-43010 (1). The transmitter, antenna, height finder, and MTI (moving target indicator) equipment are treated by different authors in separate sections of the report. Part I includes a description of the other units of the system, some theoretical range calculations, and the detection ranges obtained with the radar at the Chesapeake Bay Annex (CBA) of the Laboratory using a small antenna approximately at ground level.

Since about 1950 the Naval Research Laboratory has been studying the possible advantages of the 200 and 400 Mc frequency bands for long-range early-warning radar systems, particularly for shipboard use (2). Prior to that time, the 1300-Mc band was generally favored for shipboard applications and the 3000-Mc band for airborne early warning. A study of the relative merits of frequencies in the 100 to 500 Mc band for search applications has been presented in an appendix of a recent NRL report (3).

In 1953, when the Navy acquired the responsibility of providing offshore radar barriers for continental air defense, the Office of Naval Research suggested that airships fitted with large internally mounted antennas might prove to be effective AEW vehicles. A study (4) by NRL of 40, 100, and 200 Mc systems suggested that these frequencies possess certain advantages for such airborne radars. Later the same year, NRL and Lincoln Laboratory engaged in a joint project to investigate the lower frequencies for AEW applications (5). The frequency which was chosen for investigation was 425 Mc, a compromise between the 1300 and 200 Mc bands proposed by Lincoln Laboratory and NRL respectively. An experimental radar was assembled and flown, with excellent results, in a ZPG-2 airship at Naval Air Development Unit (NADU), South Weymouth, Massachusetts.

An extension of these experiments was the investigation (6,7,8) of height-finding by utilizing the sea-reflection interference lobe structure. This work was carried out by NRL during 1954 in conjunction with NADU personnel.

In May 1954 the Naval Research Laboratory recommended the construction of an experimental airborne radar at 220 Mc. This frequency offers certain advantages over the 400-Mc band:

1. The sea appears smoother, so that interference lobes are better defined. This favors height-finding by lobe-counting.
2. Sea clutter should be less severe.
3. The antenna is simpler, and its tolerances less critical.
4. The vertical coverage is adequate without antenna stabilization.

On the basis of range performance only, there is no great difference in radars at these two frequencies when the systems operate with antennas of equal area and transmitters of equal power.

As a result of this recommendation, the Bureau of Aeronautics established problem NRL-EL-43010 calling for the design and construction of a complete 220-Mc radar system with a 17-1/2 x 4 foot antenna. In addition, the Laboratory was to furnish the design of a 33-1/2 x 9 foot antenna for internal mounting in a ZPG-2W airship.

PART I - THE RADAR SYSTEM AND TEST RESULTS

R. L. Eilbert and A. M. Knopp

The radar system was constructed using components of an AN/APS-20E AEW radar as much as possible. Major additional tasks were the design and construction of (a) the antennas, (b) a new transmitter and duplexer, (c) the height-finding equipment, and (d) an MTI (moving target indicator).

The system was first installed with the 17-1/2 x 4 foot antenna at CBA, where ground tests were conducted to evaluate overall system performance. Except for the antenna, the system was then removed to Akron, Ohio, for installation in the ZPG-2W airship along with the 33-1/2 x 9 foot antenna. This installation has been completed by the Goodyear Aircraft Corporation, and the following research program will be carried out:

1. A check of the range performance of the system against theoretical predictions.
2. An investigation of the lobe-counting method of height-finding at 220 Mc.
3. An extension of the existing knowledge of sea clutter at this frequency.

RANGE COMPUTATIONS

Performance calculations have been made for the system to be operated in the airship. Similar calculations were also made for the system tested at CBA.

The 50% blip/scan range for a scanning pulsed search radar may be defined as the range at which the probability that a detectable echo signal will be received during a scan is 50%. The calculation of this range is based on the reflection characteristics of the target (radar cross section), the radar parameters, and certain propagation factors.

The range at which a 50% blip/scan ratio can be expected is

$$R_{50} = 176.4 \left[\frac{P_t \; G_t \; G_r \; \sigma_{50} \; L_t \; L_r \; L_p \; L_a \; F^4}{f^2 \; \overline{NF} \; B \; V} \right]^{1/4}$$

where

P_t - transmitted pulse power in kilowatts

G_t, G_r - antenna power gains, transmit and receive respectively

σ_{50} - median value of the radar cross section in square meters (the value which, as σ fluctuates, is exceeded 50% of the time)

L_t, L_r - transmission line and duplexer loss, transmit and receive respectively

L_p - antenna pattern-loss factor

L_a - atmospheric attenuation

F - pattern-propagation factor excluding attenuation

f - radar frequency in megacycles

$\overline{NF}$ - receiver noise figure

B - receiver pre-detection bandwidth in kilocycles

V - visibility factor (or minimum detectable signal-to-noise power ratio for 90% probability of detection).

The visibility factor depends primarily on the number of pulses integrated by the observer, or, for a conventionally scanning radar, the number of pulses per beamwidth, which equals $\theta \cdot \text{prf}/6 \cdot 1/\text{rpm}$. Neglecting the correction for sweep speed, which is not a factor here,

$$V = V_{opt} + 10 \log\left[\frac{1}{4}\left(1 + \frac{1.2}{B\tau}\right)^2\right]$$

in which B is the receiver pre-detection bandwidth in cycles per second, τ is the pulse duration in seconds, and V_{opt} is the visibility factor for the condition of optimum bandwidth.

The parameters of the radar to be installed in the airship are

P_t = 750 kw

τ = 5 μ sec

G_t = 22 db

G_r = 22 db

L_t, L_r = 1.0 db total

L_p = 1.6 db

L_a = 0 db

f = 220 Mc

$\overline{NF}$ = 4 db

B = 300 kc

θ_h = 7.9 degrees

θ_v = 25.7 degrees

Antenna rotation rate = 6 rpm

V = -0.715 db

The value of F, the pattern propagation factor, is a function of the amount of divergence encountered at a particular target (because of the effect of the earth's curvature on the reflected wave) as well as the spatial position of the target within the lobe pattern. The method used to calculate the effects of divergence is described by Kerr (9). This analysis will be restricted to points in space lying along the lobe centers. This means of course that the 50% blip/scan ranges derived are applicable only to targets located on the centerline of a lobe. Targets flying at altitudes less than that at which this 50% blip/scan range occurs will be detected at shorter ranges.

With the antenna at a height of 3000 feet, the 50% blip/scan ranges for a one-square-meter target at various lobe centers are shown in Table 1. These values are plotted on a range-height diagram in Fig. 1.

TABLE 1
Calculated 50% Blip/Scan Ranges
for an Antenna Height of 3000 Feet

Lobe	F	Range (naut mi)	Target Altitude (ft)
1	1.33	179.0	11,100
2	1.44	192.5	16,300
3	1.49	200.3	20,000
4	1.54	207.0	23,200
5	1.57	212.0	25,750
7	1.63	218.3	30,700
11	1.71	230.2	40,000
25	1.86	248.0	63,000

The radar parameters of the system tested at CBA which differ from those listed above are:

P_t = 640 kw

G_t = 16 db

G_r = 16 db

θ_h = 19.3 degrees

$\theta_v \cong$ 50 degrees

Antenna rotation rate = 5 rpm

V = -3.42 db.

[redacted]

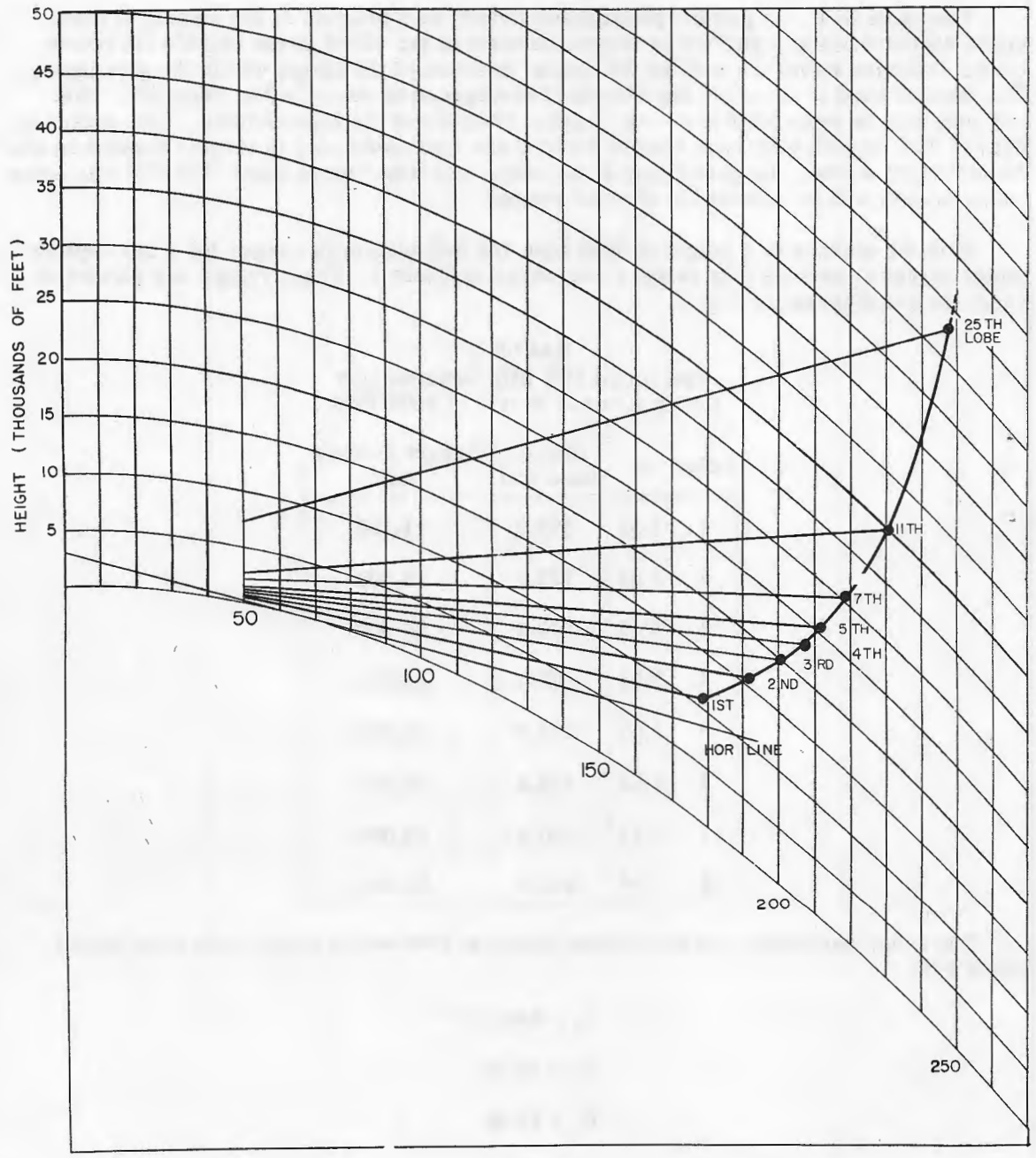

Fig. 1 - Theoretical coverage diagram. Locus of calculated values of R_{50} on lobe centers for an antenna height of 3000 feet

For an antenna height of 113.5 feet (which is essentially at ground level) the value of F on the lobe center is practically 2, since the effect of divergence at low antenna heights is negligible. Thus, using the parameters of the radar at CBA, the 50% blip/scan range for a one-square-meter target is 151 nautical miles on the lobe center.

Dynamic measurements of target cross-sectional areas have been made at NRL(10,11). The values obtained at 220 Mc for the FJ-2 are 2.5 square meters, nose aspect, and 1.5 square meters, tail aspect. A considerable increase in effective area was reported for a small change in aspect. The FJ-3, one of the aircraft used in the CBA trials, is dimensionally similar to the FJ-2. Predicted ranges using these cross-sectional areas result in a 50% blip/scan range of 167 nautical miles for the FJ-3, tail aspect, and 189 nautical miles, nose aspect.

No dynamic target cross-section measurements have been made for the F9F-8 aircraft. Although a rough estimate of 1.5 square meters cross section at 220 Mc for an F9F was used by L. V. Blake (12), this report will make no effort to establish the cross-sectional area of the F9F-8. Instead, to make a rough comparison between predicted and experimental ranges, the 50% blip/scan predicted range will be presented for both a one-square-meter target and a five-square-meter target.

AIRSHIP CONSIDERATIONS

The Goodyear Aircraft Corporation has been working in close collaboration with the Naval Research Laboratory on the technical problems encountered in the airship installation of the radar. Figure 2 shows the antenna suspended from a newly installed platform. This platform (approximately five feet by twelve feet with sloping sides) is hung from the top of the envelope. Access to this platform is made via the AN/APS-62 height-finder radome and an 80-foot tunnel which connects the radome to the car of the airship.

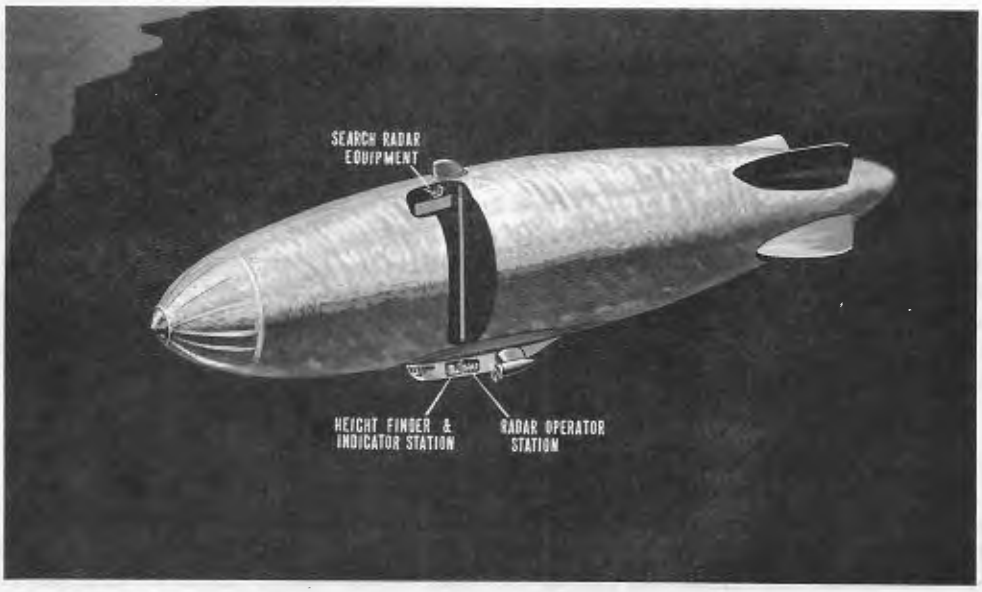

Fig. 2 - Drawing of the ZPG-2W airship showing radar-system location

On the platform will be located most of the major radar components, such as transmitter, modulator, high-voltage power supply, duplexers, and receiver. Only the control system, indicators, height-finding, and MTI equipments are located in the car. The receiver can be remotely tuned, but not the transmitter.

Goodyear has assumed the following major assignments:

1. To determine and make the necessary structural changes required in the ZPG-2W airship.
2. To determine the mechanical design and construct the large antenna.
3. To design and construct the antenna pedestal.
4. To design and construct the dual rotary joint (radar and IFF).
5. To design and construct the servo control system, including a hand-slew control for searchlighting, and north stabilization equipment.
6. To provide all external interconnecting cables between units.
7. To make the complete radar system installation.

DESCRIPTION OF EQUIPMENT

The transmitting portion of the vhf radar system consists of a special oscillator utilizing the Eimac 3W10,000A3 triode, fed by a line-type modulator employing dc resonant charging. The antenna used for the trial runs at CBA is a 17-1/2 x 4 foot, 14-element dipole array. These designs are described in Parts II and III respectively.

In addition to the normal radar system functions, the equipment includes two special units necessary to the 220-Mc research program for which the system was designed: (a) a height finder, comprising a tracker unit and a recorder unit, which measures the number of interference lobes per mile traversed by the target and (b) a noncoherent clutter-gated MTI unit. These units are described in Parts IV and V respectively.

In the following description of the other units of the vhf system, those units incorporated intact from the APS-20 radar are mentioned only briefly. Detailed descriptions may be obtained in the AN/APS-20B instruction manual (13,14). Units of the APS-20 which have been modified are described without details of the functioning of the unit, since this is in most cases similar or identical to that of the original. For the units designed especially for the vhf system, more comprehensive details are given. A functional block diagram of the system is shown in Fig. 3.

The Synchronizer

The synchronizer remains fundamentally the same unit as the SN-55/APS-20B. The repetition rates provided by that unit were 900 and 300 pps. Changes have been made to alter the basic pulse rate from 900 pps to 600 pps. This change had been planned with the original intent of providing operation of the system at either of two repetition rates, namely, at 600 pps or at 300 pps. At a later stage of system planning, the higher repetition rate was abandoned. Thus 300 pps is the only repetition rate available and is obtained

from the 600 pps and count-down circuits in this unit. Of the various other functions of the original equipment the following are preserved intact: circuits for the coding and transmission of information through the relay link; azimuth information for the indicators; range and heading marks for the indicators. The sector-scan control circuits have been disabled.

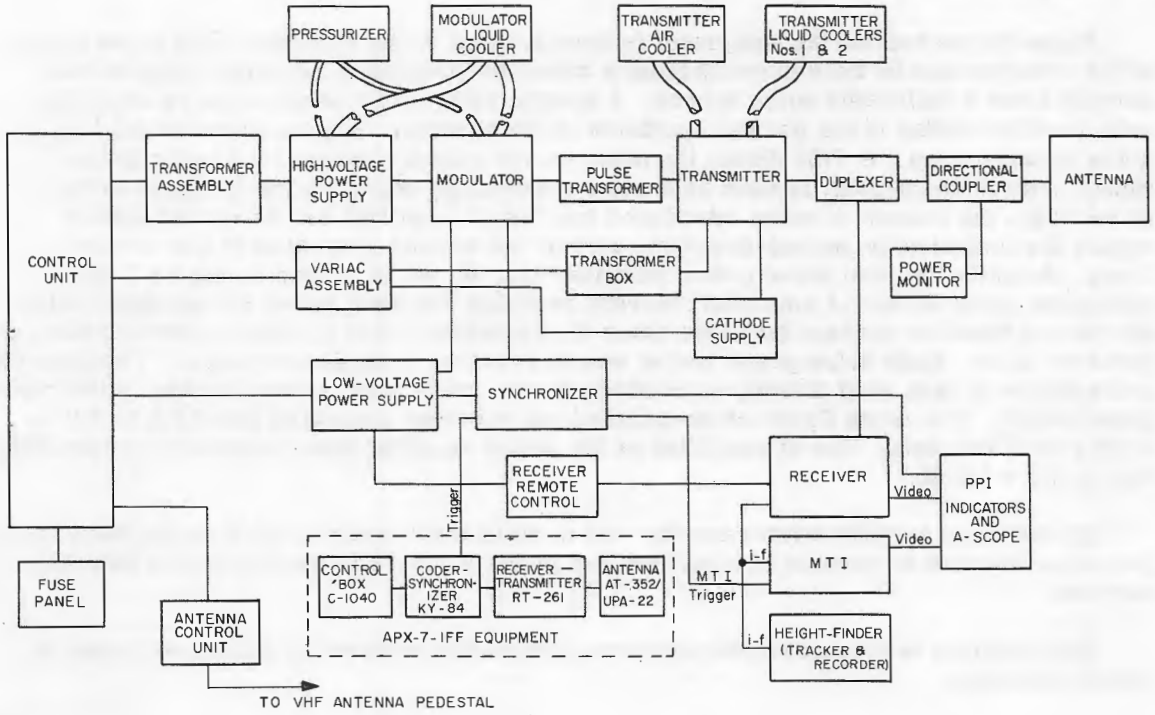

Fig. 3 - Functional block diagram of the vhf system

The Low-Voltage Power Supply

The low-voltage power supply has been changed chiefly by the addition of a circuit to supply +250 volts regulated dc. Circuitry for the negative 255-volt supply is still intact although the voltage is no longer brought to the external connectors. The other voltages supplied by this unit remain the same as in the original equipment (PP-347/APS-20B).

The Receiver

The radar receiver first designed for this system, and used in the CBA tests, employed a type 416 tube as an rf amplifier. It was found, however, that because of the nature of the mounting, considerable difficulty was involved in changing tubes. As a result a new receiver is being built with a low-noise 215 to 220 Mc converter (15) employing GL-6299 tubes in a two-stage rf amplifier. These tubes are more easily replaced and, in addition, require no forced-air cooling.

The i-f preamplifier and the i-f and video amplifiers of the APS-20 are on separate chassis. These are used in the vhf system with minor changes. The input circuit of the i-f preamplifier has been altered. In the i-f amplifier the bandwidth has been narrowed to 300 kc, a cathode follower has been included to supply i-f to the MTI unit, and the second detector has been changed to a 1N34 crystal. The beacon and MTI circuits on the video amplifier are not used although the circuitry remains intact.

Noise-figure measuring equipment is incorporated in the receiver. The noise figure of the receiver can be read directly from a meter by comparing receiver noise to that derived from a calibrated noise source. A coaxial relay at the input of the rf amplifier selects either radar rf for normal operation of the receiver or noise diode output for noise measurement. A 5722 diode, the noise-power output of which is directly proportional to its plate current, is used as a noise source. By adjusting the filament voltage of the 5722, the amount of noise introduced into the rf amplifier can be varied until it equals (as indicated by second-detector current) the amount generated in the receiver itself. Actually the total noise power (receiver plus diode) is passed through a 3-db attenuator prior to the i-f amplifier, thereby reducing the input power by one-half. When the second detector current for diode noise plus receiver noise is equal to that for the receiver alone, diode noise-power output equals receiver noise-power output. The receiver noise figure is then read directly in decibels from a calibrated microammeter in the diode plate circuit. The noise figure of the original vhf receiver measured about 3.5 to 4.0 db during the CBA tests. The rf amplifier of the newer receiver has a noise-figure specification of 3.0 ± 0.2 db.

By means of another microammeter and a multicircuit wafer switch on the front panel, provision is made to monitor rf amplifier and mixer plate currents and second detector current.

The receiver is located on the platform close to the duplexer to minimize losses in the rf input line.

The Receiver Remote Control Unit

The receiver remote control unit can control all of the previously mentioned functions of the receiver at the operator's station in the car of the airship. The remote control unit also has controls for i-f gain, STC, IAGC, and rf and local oscillator tuning.

The Transformer Assembly

The transformer assembly contains the motor-driven three-phase autotransformer and associated control circuitry for varying the input power to the high-voltage power supply. This unit is the TF-158 transformer assembly of the APS-20 radar with the magnetron filament circuitry removed.

The High-Voltage Power Supply

The high-voltage power supply which supplies dc power at a maximum of 13 kv and about 300 ma to the modulator also was originally a unit of the APS-20 (PP-829/APS-20B). The only change made was the addition of a resistance network for monitoring the dc output voltage.

The Modulator

The modulator of the vhf system is of line-type design employing dc resonant charging. The T-202/APS-20E unit is used with a number of changes necessitated by the design parameters of the new system. The magnetron and its mounting were removed from the unit. A new pulse-forming network was installed to provide a 5-μsec pulse at a repetition rate of 300 pps. The transformer subassembly which contained the magnetron and diode filament transformers, the charging choke, and the pulse transformer was replaced by a new component which includes the charging choke and diode filament transformers. The pulse transformer is now a separate unit. Retained in the modulator are the 5948/1754 hydrogen thyratron and associated circuitry, and the modulator trigger amplifier.

The Pulse Transformer

The pulse transformer is described in the transmitter section of this report.

The Variac Assembly

The variac assembly contains the manually operated autotransformers which control the cathode and filament power to the transmitter. The filament unit is a single-phase autotransformer. A cam on its shaft accuates a snap-action switch when the transformer is in the zero voltage position. This cam-switch circuit is designed to protect the cold transmitter filament from excessive initial-current surges by assuring that the filament control is turned to zero before the filament supply is energized.

The cathode supply control consists of a three-phase autotransformer. It operates a snap-action switch in a manner similar to that described above to assure that the cathode voltage is always applied gradually.

The Transformer Box

The transformer box contains the filament transformer for the 3W10,000A3 transmitting tube. It is energized from the filament Variac described above. This transformer is current-limited so that its secondary will saturate under short-circuit conditions at 50 amperes, which is the specified maximum filament current of the transmitting tube. In the transformer box are current and potential transformers and meters for monitoring the filament. The potential transformer is necessary because the filament can be at a dc potential as high as 3000 volts negative with respect to ground. Also located in this unit are the keep-alive voltage-supply for the duplexer TR tube and a timer to record hours of operation of transmitter radiation.

The Cathode Supply

The cathode supply is a high-voltage power supply providing a maximum potential difference of 3000 volts at 2.5 amperes between the cathode and filament of the 3W10,000A3 transmitting tube. The output of this selenium-rectifier supply is controlled by the three-phase autotransformer in the Variac assembly. This unit also contains a timer for registering hours of operation of the 3W10,000A3 cathode, relays for load protection, and circuitry for metering voltage and current of the supply.

[redacted]

[redacted]

The Fuse Panel

The fuse panel houses the main power fuses and circuit overload breakers for most of the units of the system.

The Antenna Pedestal and Control Unit

The antenna control system used in operating the vhf system at CBA is designed to provide both searchlighting control and continuous scanning of the antenna. The antenna pedestal (formerly AS-407/APS-20B) was modified by changes in circuitry to adapt to the new control system and by the substitution of a 3-1/8-inch rotary joint for operation at the power level of the 220-Mc system without pressurization. This is a dual rotary joint, providing for the IFF antenna as well as the vhf antenna.

The antenna control unit contains a servo control circuit using two type 6044 thyratrons. The error-signal inserted by means of a 400-cps servo control transformer is limited, rectified, and amplified for application to the grids of the thyratrons. Also contained in this unit are controls for continuously scanning the antenna pedestal at 5 rpm. This was the maximum speed that could be obtained by the 28-volt dc motor with the relatively heavy load presented by the 17-1/2 x 4 foot antenna. The antenna control system to be used with the vhf system on the airship will be designed and built by Goodyear Aircraft Corporation. In addition, the new antenna control system will incorporate north stabilization.

The A-Scope and Power Supply

The A-scope is a converted ASB-7 indicator. The sweep circuits of the original equipment were modified to convert from a B display to an A display. A video amplifier was added to the circuit. The A-scope power supply was built to furnish the dc and filament voltages required by the indicator.

The Control Unit

The control unit contains most of the major switching, control, and monitoring functions of the vhf radar system. This unit, together with the receiver remote control, Variac assembly, and antenna control is located at the operator's station in the car of the airship, and provides centralized control for the entire system. Ten panel meters on the control unit monitor the following system parameters: filament current and voltage of the transmitting tube, cathode-supply current and voltage, modulator current, high-voltage-power-supply voltage, plate and grid current of the transmitter, and the dc and ac line voltages.

An interlock system is incorporated for protection of the high-voltage portion of the radar, and for the protection of personnel. The interlock circuit protects equipment against damage by preventing improper application of tube voltages and assuring proper operation of the cooling system before high voltage is applied to the transmitter, modulator, and high-voltage power supply.

The control unit also contains indicator lamps for checking the operation of various components and functions of the system. Controls located on the front panel consist of power switches, controls for energizing the high voltage and varying the level of radiation, an overload reset switch, and the MTI controls.

[redacted]

Other Equipment

Other units, which are standard and have been incorporated without change into the vhf system, are listed below with their commercial designations or military equipment classification numbers:

1. Indicator, range and azimuth, IP-203/APS-20B
2. Indicator, range and azimuth, APA-113
3. Pressurizer (air compressor), HD-126/APS-20B
4. Liquid coolers for modulator, high-voltage power supply, and transmitter, HD-125/APS-20B
5. Transmitter air cooler, Rotron duplexer blower; output capacities 35 and 85-100 cfm, NRL contract No. 2489-56
6. Power monitors, Hewlett-Packard, model 430-C.

Other equipment used in conjunction with, but not a part of, the vhf system consists of:

1. IFF equipment, AN/APX-7
2. IFF antenna, AT-352/UPA-22
3. Radio transmitting set, AN/ART-28

The total weight of the vhf system, including height-finding and MTI equipment but not IFF, is approximately 2200 pounds.

INSTALLATION

The vhf radar system with its associated equipment was installed in a trailer for the initial tests at CBA. The vehicle used was a stripped-down equipment trailer, type CAHU-10301, a part of the SP-1M radar equipment. This arrangement had the advantage of allowing the equipment installation to be performed at the Laboratory within access to shops and supply, and also provided means for transporting the equipment to CBA and then to the Goodyear Aircraft Corporation at Akron, Ohio, without dismantling it. (Goodyear required use of the system prior to installation of the equipment in the airship to make the high power tests on the 33-1/2 x 9 foot antenna.) Various views of the equipment installed in the trailer are shown in Fig. 4.

The antenna was installed on a platform at CBA overlooking the bay, as shown in Fig. 5. The height of the antenna, measured from its centerline, was 113.5 feet above mean sea level. An APS-20 radome was set up in an inverted position surrounding the antenna and pedestal assembly, affording them some measure of protection from the weather, while simulating the conditions under which such an antenna would operate. The top opening in the radome was covered by a tarpaulin when the system was not in use.

The rf line from the rear of the trailer was fed into the antenna pedestal through approximately 25 feet of 3-1/8-inch rigid coaxial transmission line. There were three bends in the rf line outside the trailer and three inside. The IFF antenna mounted on top of the 17-1/2 x 4 foot antenna at CBA was connected to the AN/APX-7 IFF equipment in the trailer through a length of RG-8/U flexible coaxial transmission line.

[redacted]

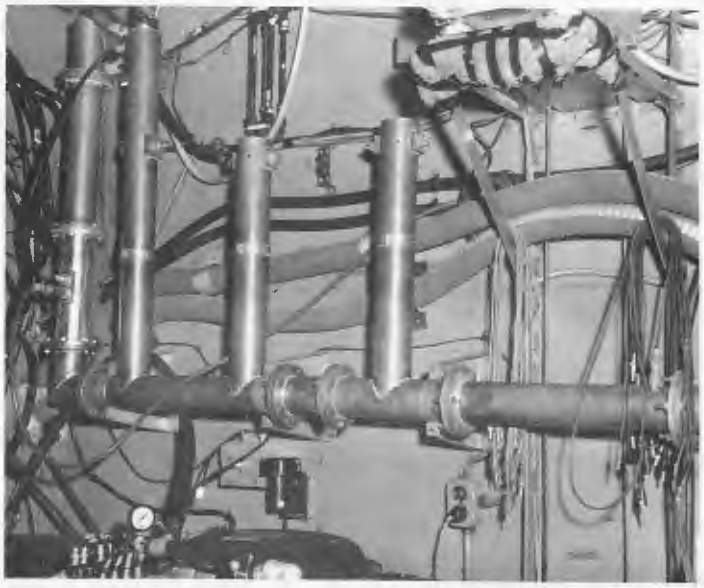

(a) Directional coupler, duplexer, and auxiliary ATR installed in the rf line

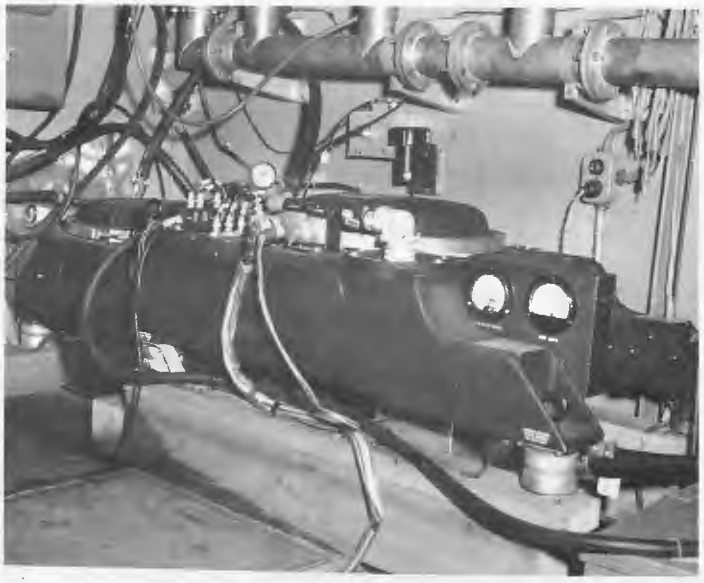

(b) High-voltage power supply and modulator

Fig. 4 - Equipment installed in the trailer at CBA

(c) Transmitter assembly with tuning stubs and type OA-2 frequency meter

(d) Operator's control station

(e) Equipment station

Fig. 4 - Equipment installed in the trailer at CBA

(a) Radome and equipment trailer

(b) Antenna-radome assembly

Fig. 5 - Installation at CBA overlooking the Chesapeake Bay

OPERATION

The vhf radar system was operated daily for nearly two months at CBA during May and June 1956. Test flights were obtained occasionally during this time. Several major difficulties were encountered:

1. It became apparent after several test flights that the maximum ranges were considerably below theoretical expectations. A possible cause of this trouble was indicated by the noticeable decrease in noise on the A-scope when the transmitter was de-energized. Measurements of minimum detectable signal at the receiver output for various excitation conditions of the transmitting tube (high voltage on, off; cathode supply on, off; filament on, off) showed that this noise was being introduced by the action of cathode bombardment. The noise was reduced about 6 db by the addition of an auxiliary ATR inserted in the transmission line between the transmitter and the duplexer. A definite improvement in radar range performance was obtained after this change.

2. The cathode supply was found capable of maintaining current flow in the transmitter cathode long after the filament had been de-energized. An interlock had been provided to de-energize the filament in the event of a cooling-system failure; cathode current was expected to decrease to zero automatically. When this did not occur, the resultant build-up of heat in the transmitter caused damage to the tube and the cooling hoses. This trouble was remedied by the addition of a separate cooling-system interlock to de-energize the cathode supply.

3. During initial operations at CBA the radar interfered with communications and other test equipment on the base. This occurred when the antenna was directed at various buildings as it revolved. To prevent this interference, a sector switch was inserted in the system. This consisted merely of a coaxial relay which connected the trigger to the modulator for the 120 degrees of rotation during which the antenna was directed toward the bay. The relay was operated by a 28-volt dc signal from a set of relays and cams already extant on the pedestal assembly. The system was operated at a reduced pulse power of 640 kw when the sector switch was being used, because the voltage of the unloaded high-voltage power supply rose to its maximum allowable value at this power setting.

GROUND TESTS

For the performance tests at CBA, jet aircraft were flown at altitudes of 20,000, 30,000, and 40,000 feet on a true bearing between 30 and 50 degrees. Data were recorded from the presentation on an APS-20 PPI indicator. A calendar of flights is presented in Table 2. Flights made prior to May 31 are not listed. This was the period, as explained above, during which noise generated in the transmitter cathode caused inadequate range performance.

IFF was used as often as possible during the flights. It proved a very definite aid in distinguishing the test aircraft from the many other air targets in the vicinity, particularly when the aircraft strayed from the designated course. On many occasions, unfortunately, either the plane did not have the necessary IFF equipment or, if it did, the equipment was not functioning properly. This is the explanation for such notations in Table 2 as "wrong plane followed" and "plane never located." The MTI unit, planned as part of this system, was not available at the time of the CBA trials.

[redacted]

TABLE 2
Calendar of Flights at CBA

Date and Time	Aircraft	Altitude (ft)	Flight Direction	Remarks
May 31 - am	F9F-8	20,000	Out and in	Data incomplete because of troubles in video amplifier.
May 31 - am	F9F-8	20,000	Out and in	
June 4 - am	F4-D	40,000	Out and in	Data inconclusive. Water was found in coaxial line at start of first run. Radar was operated at reduced power for remainder of these two runs.
June 4 - am	F4-D	40,000	Out and in	
June 4 - pm	F4-D	30,000	Out and in	
June 5 - noon	FJ-3	40,000	Out and in	
June 5 - pm	FJ-3	30,000	Out and in	
June 7 - am	FJ-3	20,000	Out and in	
June 7 - pm	FJ-3	20,000	Out and in	
June 8 - am	FJ-3	30,000	Out and in	
June 11 - am	FJ-3	40,000	Out and in	
June 11 - pm	FJ-3	40,000	Out and in	
June 12 - am	FJ-3	30,000	Out and in	
June 15 - pm	F4-D	40,000	Out and in	Transmitter operated at 800-kw peak power.
June 18 - pm	F9F-8	30,000	Out	No data - wrong plane followed.
June 18 - pm	F9F-8	30,000	In	
June 22 - am	F9F-8	30,000	Out	Transmitter operated at 800-kw peak power.
June 22 - am	F9F-8	30,000	In	No data - receiver inoperative.
June 22 - pm	F9F-8	30,000	Out	No data - plane never located.
June 22 - pm	F9F-8	30,000	In	

RESULTS

The results from flights of various jet aircraft are presented in the form of blip/scan histograms (Figs. 6,7,8). In computing these blip/scan ratios, the number of times a target is seen on the PPI is expressed as a percentage of the total number of scans as the target moves through a range interval arbitrarily taken as five miles. The data from test flights with the same aircraft at the same altitude are averaged together. Because of the various types and limited number of aircraft available, nearly half of the histograms represent the data for single runs only.

On these histograms are shown the ranges at which the calculated maxima and minima of the first three lobes occur at the particular altitude under consideration. The centerline of the first null is coincident with the horizon line of the radar.

Analysis of the data beyond actual presentation in the form of blip/scan curves is subject to certain limitations, particularly since the limited number of flights conducted does not provide sufficient data to present a statistical sample on which comparisons can be based. The value of σ_{50} is subject to much conjecture, which also causes the predicted 50% blip/scan ranges to be limited in accuracy. Because of the lack of knowledge of the value of σ_{50}, the blip/scan curves have been presented with the predicted 50% blip/scan range indicated on each curve for a one-square-meter target, and for a five-square-meter target.

Since the most reliable value assumed for any of the aircraft were those of the FJ-3 (these values were based on experimental determination of the cross-sectional area of the FJ-2 (10,11) which is similar to the FJ-3), these additional predicted 50% blip/scan ranges are also shown on the blip/scan curves in Fig. 6. In all the histograms of the outbound runs of the FJ-3 the blip/scan ratio is below 50% for the first lobe even when that lobe is well within the calculated 50% blip/scan range of 167 nautical miles. The data indicate a 50% blip/scan range of about 130 nautical miles for the tail aspect of the FJ-3. This could mean that the target area is less than that assumed, that radar performance was not optimum, or that certain propagation effects were encountered. In any event, insufficient data were obtained to determine the cause of the discrepancy.

Figure 9 presents the data from individual flights of an FJ-3 aircraft at various altitudes. Relative echo intensities are plotted on lines representing constant altitudes above the curved surface of the earth. The radial lines represent the calculated maxima and minima of the sea-reflection lobe pattern. Clearly shown in this diagram are the variations of signal strength caused by the aircraft traversing the various lobes. It is these variations on which the height-finding system operates. Since the antenna installation at CBA was essentially at ground level, the angle between lobes is too wide to give enough fluctuation for effective use of the height-finding method. For this reason the height-finding equipment was not employed in the CBA tests. With the system installed on the airship and flying at an altitude of several thousand feet, however, the pattern will contain a larger number of lobes more closely spaced, thus facilitating accurate height determination.

It can be seen by reference to Fig. 9 how detection range is limited by the location of the maximum of the lowest sea-reflection interference lobe in relation to the target altitude. Thus the data presented here give no precise indication of the value of this 50% blip/scan range. The observed ranges can be extrapolated, however, to obtain a value for this range which is applicable to a target flying always in the center of the lobe. This has been done with the outbound data of Fig. 9 and the value thus obtained for the FJ-3 is 220 nautical miles. The actual ranges obtained in the tests at 20,000 and 30,000 feet were 161 and 194 nautical miles respectively.

Figures 10 and 11 are photographs of the radar presentation as viewed on an IP-203/APS-20B indicator. In Figs. 10a, 10b, and 11a the arrows locate the target aircraft (an FJ-3) at different ranges during the course of one of the flights. Figure 11b shows a random target at 187 nautical miles. These chance targets were seen at various times at distances as great as 230 nautical miles (the end of the sweep on the PPI). Although their exact nature is unknown, these random targets were certainly aircraft of some type.

FUTURE PLANS

It is anticipated that some maximum-range information and height-finding data will be obtained with the 220-Mc radar system during June 1957. At that time Goodyear Aircraft Corporation is scheduled to commence the Navy acceptance tests for the ZPG-2W airship. More complete data will be taken after August 1, 1957 when the airship will have been delivered to NADU, South Weymouth, Massachusetts. This data will include the performance of the radar, its comparison with predicted results, and comparison with radars operating at other frequencies, if these radars are available. For example, comparison may be made with the AN/APS-20E and the AN/APS-70 radars.

The potential advantages of this system with respect to the effects of sea clutter will also be investigated. Plans have been made to measure the scattering cross section of the

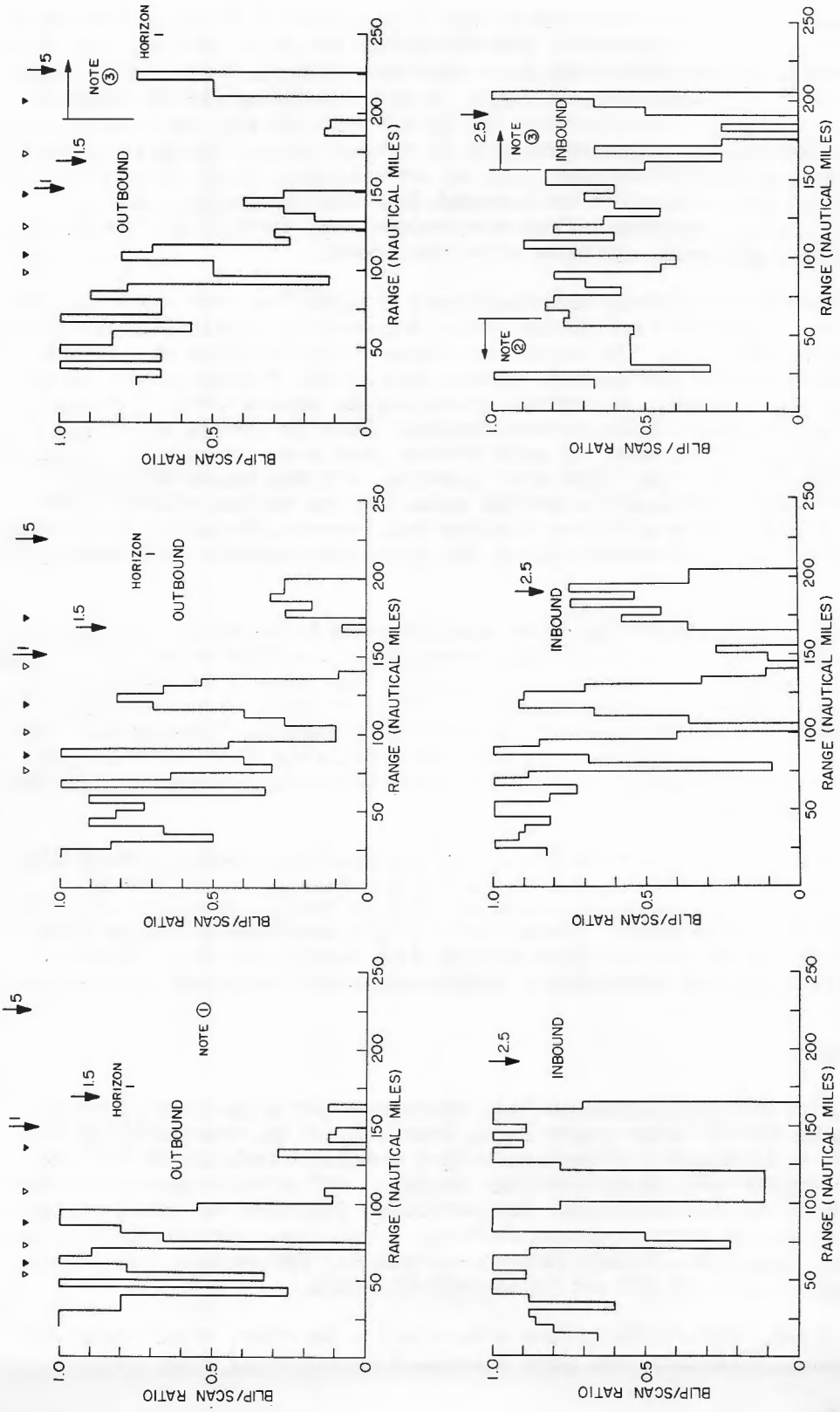

NOTES

① RECEIVER REQUIRED RETUNING ON PM RUN

② FLIGHT OF 11 JUNE (PM) LOST AT 60 MILES PLANE WENT OFF COARSE DURING A NULL.

③ DATA FROM SINGLE RUN -- 11 JUNE (AM)

Fig. 6 - Histograms of blip/scan ratios for an FJ-3

The open triangles indicate the ranges at which minima occur and the solid triangles maxima for the first three lobes. Predicted ranges for various cross sections (square meters) are in-

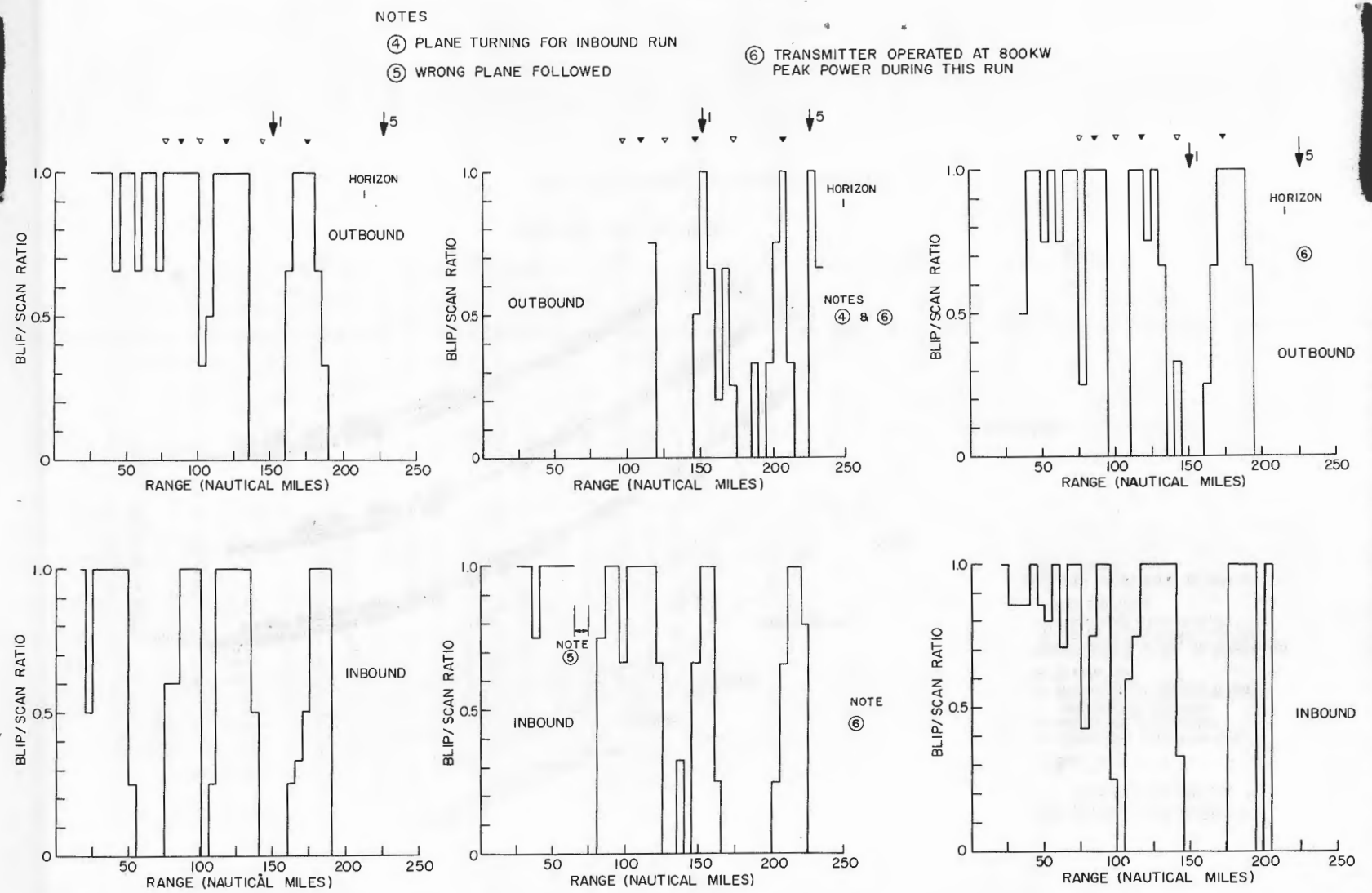

Fig. 7 - Histograms of blip/scan ratios for an F4-D

Fig. 8 - Histograms of blip/scan ratios for an F9F-8

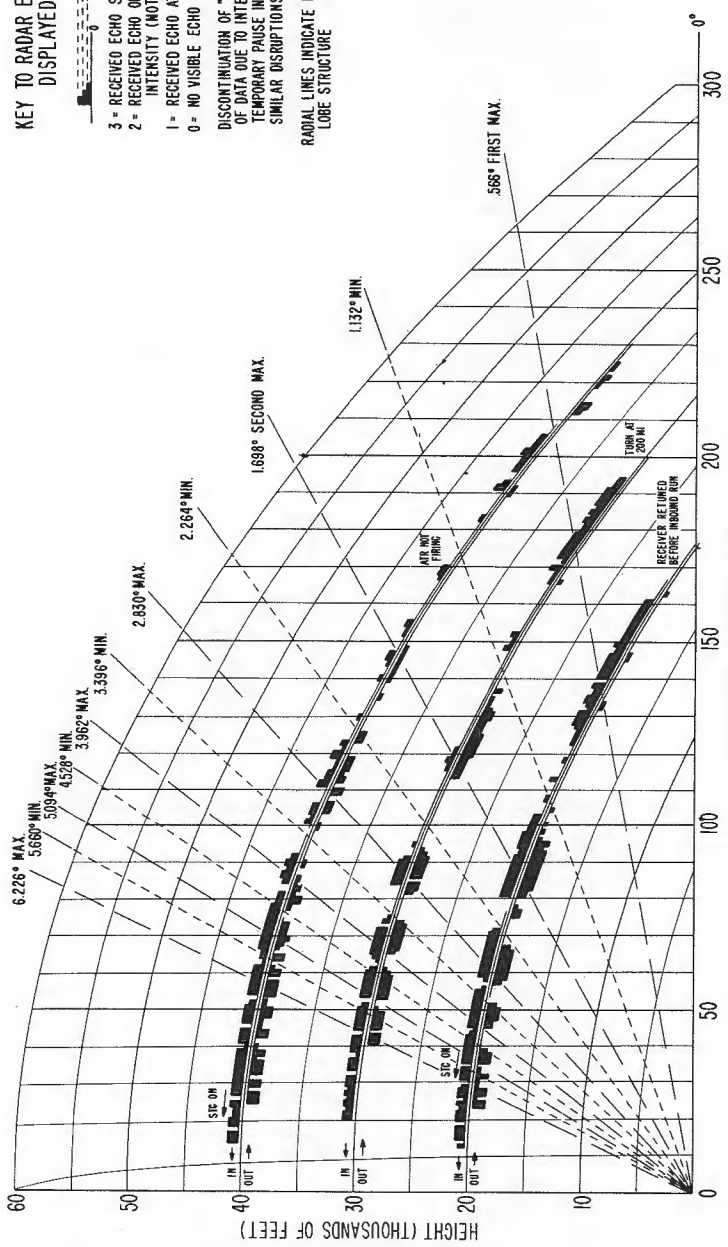

Fig. 9- Radar coverage diagram

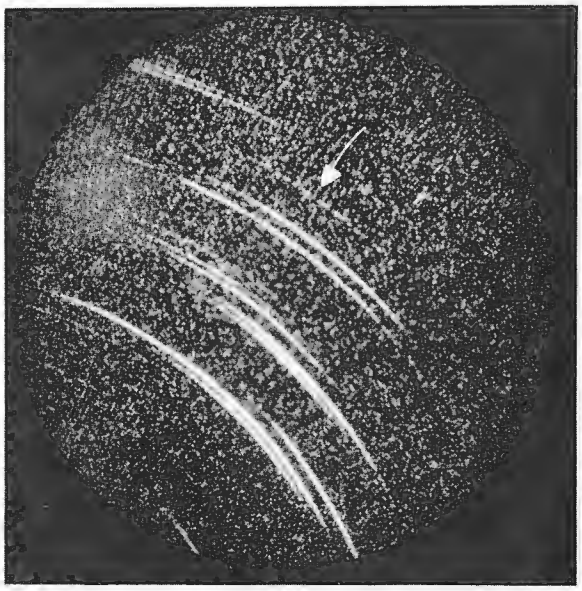

(a) FJ-3 (30,000 feet, inbound) at 130 nautical miles (see arrow)

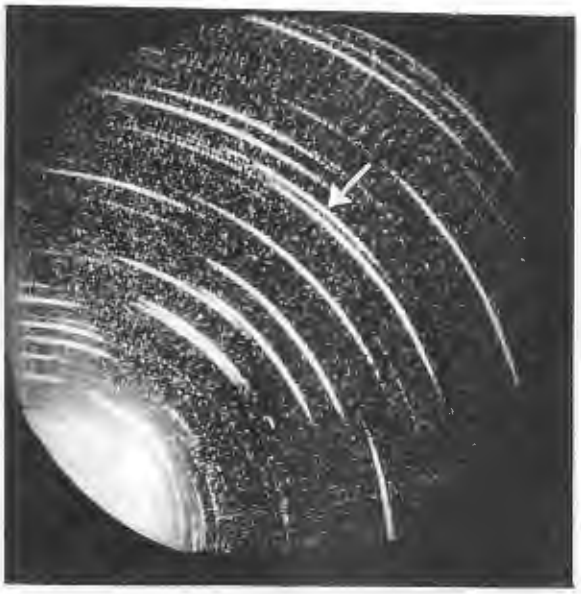

(b) FJ-3 (30,000 feet, outbound) at 85 nautical miles (see arrow)

Fig. 10 - PPI displays of the vhf radar. 50-nautical-mile sweep length; off centered in SW direction; June 12, 1956

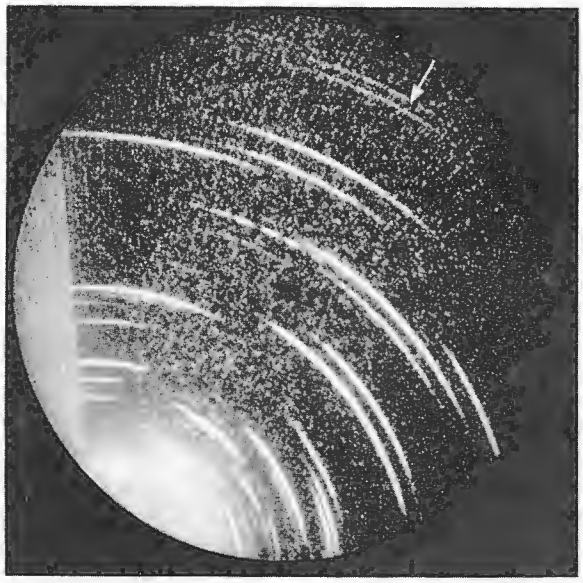

(a) FJ-3 (30,000 feet, outbound) at 110 nautical miles (see arrow). 50-nautical-mile sweep length; off centered in SW direction.

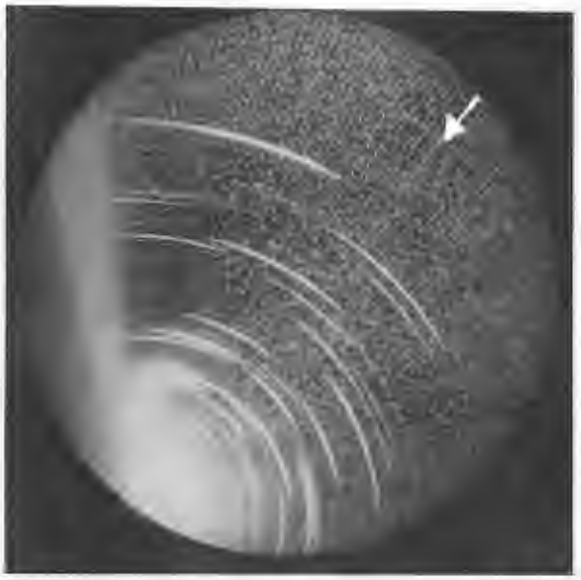

(b) Random target at 187 miles (see arrow). 100-nautical mile sweep length, off centered 100 miles SW.

Fig. 11 - PPI displays of the vhf radar, June 12, 1956

sea per unit area, σ_0, at various angles of illumination and under a number of sea states. Pulse-to-pulse photography will be used in making the measurements. The effectiveness of noncoherent clutter-gated MTI at this frequency will also be determined.

The height-finding capabilities of the equipment utilizing the sea-reflection, interference lobe structure will be compared with results obtained at higher frequencies, as well as with other types of systems. (It is expected that the ZPG-2W airship will be equipped with the AN/APS-62 height finder.) Data will be gathered to determine the amount of target scintillation in order to predict its effect on a proposed FM height finder (16). The effects of rough seas on the accuracy of height measurements will be studied. (Since height-finding by the lobe-counting method has been successfully demonstrated (7,8) for longer ranges than have been obtained with other airborne height-finding equipments, the Bureau of Aeronautics is presently negotiating with Goodyear Aircraft Corporation to include this type of height-finding equipment on the new and larger ZPG-3W airships which will be equipped with AN/APS-70 radars.)

[redacted]

PART II - THE TRANSMITTER

T. S. Golden

To meet the size, weight, and rf power requirements for the airborne application of this radar system, a pulsed triode oscillator was the most desirable form of transmitter circuit. The vacuum tube chosen was the Eimac 3W10,000A3. Several circuit configurations were considered and the grid bell type of oscillator was selected for development.

Briefly, the electrical characteristics prescribed for the transmitter were the following:

Frequency range - 216 to 225 Mc

RF pulse power - 500 kw minimum

Pulse length - 5 μsec

Duty factor - 0.0015

In addition to the high-power transmitter it was necessary to develop an antenna duplexer for the system. To meet these requirements a branched-line type of duplexer with 3-1/8-inch coaxial line was designed.

GRID BELL OSCILLATOR

Circuit Description

The rf circuit for the grid bell oscillator (Fig. 12) is primarily contained by a 10-inch-diameter outer cylinder about 48 inches long exclusive of mounting. In the top end of this cylinder, the vacuum tube is held in place concentrically by a blocking capacitor and an rf plate choke arrangement. This re-entrant choke grounds the anode (for rf potential) to the outer cylinder wall and at the same time isolates the plate pulse voltage from ground. A small, 2-3/4-inch-diameter, hollow metal cylinder, concentric with the outer cylinder, extends downward from the cathode stem of the vacuum tube to a rigid mounting at the bottom of the outer cylinder. Contact to and support of the cathode end of the vacuum tube is thereby provided. This smallest cylinder is referred to as the cathode line. Cathode cooling air, and filament and cathode-bombardment power, are introduced inside the cathode line.

The remaining principal part of the oscillator circuit consists of a 6-inch-diameter, thin-wall cylindrical section. This cylinder, referred to as the grid bell, is suspended at its upper end on the grid electrode of the vacuum tube, is extended downward over the cathode line, and is open-ended at the bottom. Teflon rings hold the grid bell securely in place inside the outer cylinder. The length of the grid bell is the main frequency-determining element for the oscillator. A dc grid bias connection to the grid bell along with a re-entrant rf choke to minimize leakage of rf energy via the bias lead is provided. An output coupling loop for rf loading is located in the region between the grid bell and the outer cylinder. Tuning adjustments provided consist of a telescopic variation in the length of the grid bell and a movable contacting short circuit (referred to as the cathode short) between the cathode line and the outer cylinder. Adequate air and liquid cooling as prescribed by the tube manufacturer is provided by auxiliary equipment.

[redacted]

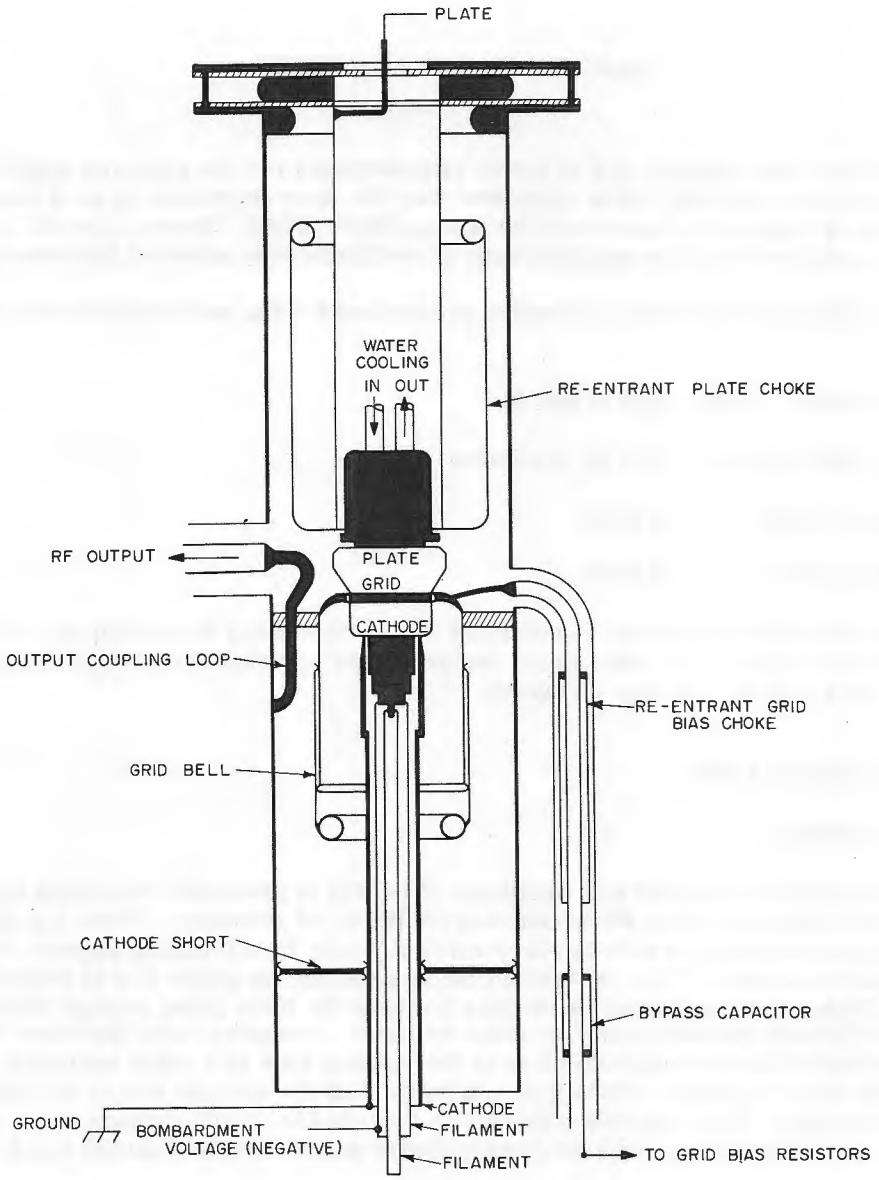

Fig. 12 - Cross-sectional view of the grid bell oscillator

Theory of Operation

The grid bell oscillator may be most easily described if one considers (a) the region between the grid bell and the cathode line extending from the open end of the bell to the grid and cathode connections of the tube as a resonant (half-wave, open-circuit) input circuit, (b) the region between the grid bell and the outer cylinder extending from the open end of the bell to the grid and plate connections of the tube as a resonant (half-wave, open-circuit) output circuit, and (c) the region between the outer cylinder and the cathode line extending from just beyond the grid bell to the movable cathode short as a feedback adjustment circuit.

Feedback for oscillation is obtained by coupling power from a high-impedance point of the output resonant circuit, through a series impedance represented by the feedback adjustment circuit, to a high-impedance point of the input resonant circuit. The discontinuity reactances at the plane of the open end of the grid bell along with the variable length of transmission line to the cathode short have a lumped equivalent circuit shown in Fig. 13 (17). In the figure, jx_1, jx_2, and jx_3 are the junction discontinuity reactions, and Z_1, Z_2, and Z_3 are the impedances looking into the output resonance circuit, the input resonance circuit, and the feedback adjustment circuit respectively at the bottom of the grid bell. The series element of the filter is adjusted by means of the variable cathode short to provide the proper magnitude and phase for the regenerative power coupled from the output circuit into the input circuit. The stability and efficiency of the oscillator are determined by these adjustments.

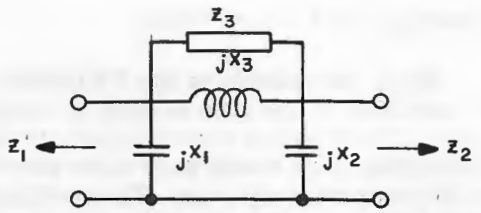

Fig. 13 - Equivalent circuit of the feedback adjustment circuit at the plane of the open end of the grid bell

ADDITIONAL EQUIPMENT

Pulse Transformer

A pulse transformer was designed which matches the 50-ohm network impedance of the modulator to the approximately 450-ohm impedance represented by the oscillator plate circuit. By means of the dc power supply, plate pulse voltage is variable up to 28 kv. Plate current reaches a pulse value of around 60 amperes under maximum loading conditions. It is important to point out that at these higher voltages soft x rays are produced inside the vacuum tube. Sufficient shielding has been built into the oscillator for normal operation. Plate voltage should never be applied to the transmitter with the access door open, however, for the protection against x-rays is lost under such conditions.

Cooling

Two sources of cooling are required. Liquid cooling for the anode is accomplished by two liquid electron-tube coolers from the AN/APS-20E system. These two heat exchangers and pumps operated in parallel provide a flow of water and ethylene glycol at approximately 4 gallons per minute. This has been found to be adequate cooling for the 3400 watts of plate dissipation (including radiated cathode power which appears at the anode of the tube).

Air cooling for the tube is provided by a duplex blower. Thirty-five cubic feet per minute at relatively high pressure (22 inches of water) is supplied through the inside of the cathode line to cool the cathode and filament seals. This air is exhausted from the oscillator enclosure through ports in the region of the feedback adjustment circuit. Another supply of air is provided at lower pressure by the same blower for cooling the glass of the grid seal. This air at a velocity of 100 cubic feet per minute enters the upper region of the output resonant circuit and is made to flow through the fingers on the grid bell which make contact to the grid electrode of the tube. In this manner the glass seal at the grid is cooled. This air, likewise, is exhausted at the ports in the region of the feedback adjustment circuit.

[redacted]

Filament and Cathode Supply

Since the cathode of the 3W10,000A3 is a bombardment-heated type, proper sequence of operation of the tube is first to raise the filament input voltage to the rated value, 10 volts. The filament transformer provided for the system is of the current-limiting type. Otherwise, care would have to be exercised in limiting the filament warmup surge current to 50 amperes maximum. The rectified 3-phase ac cathode-bombardment voltage of around 1500 volts rms (1.8 amperes) must then be applied by raising the cathode-bombardment supply Variac. After the cathode reaches operating temperature, which requires a period of about 30 seconds, the filament voltage should be reduced to around 3 volts (at 10 amperes). This is done to prevent overheating and shortening the life of the filament, since much of its heating power is supplied by radiation from the hot cathode.

Grid Bias

Grid-leak bias for the oscillator is obtained through a dc connection to the grid by way of the grid bell. Even though this connection is made at a low rf voltage point in the output resonant circuit, the provision of a re-entrant choke followed by a bypass capacitor insures against any rf leakage out the bias lead. The grid-leak resistor is made up of four woven resistor elements connected in series-parallel to provide a 350-ohm resistance with a 600-watt dissipation capability.

Output Coupling

The coupling of rf energy from the oscillator is achieved by means of a loop located in the output resonant circuit. The size and position of this loop provide the maximum coupling with the minimum risk of corona or rf breakdown from the grid bell or the anode to the loop. The output coupling line, however, must contain a double-stub tuner to match properly from the oscillator output circuit to the 51-ohm, 3-1/8-inch coaxial output line leading to the antenna.

TRANSMITTER PERFORMANCE

The variable cathode short was incorporated in the oscillator to help in the determination of the performance characteristics. It is possible that a fixed cathode short might be provided in future transmitters with a resultant small reduction in size and weight and very little sacrifice in operating efficiency.

A plot of frequency vs length of grid bell is shown in Fig. 14, and the overall efficiency (including the modulator and power supply) vs grid bell length is shown in Fig. 15. Since the modulator efficiency was about 80 percent, oscillator efficiency throughout the test was around 60 percent. In Fig. 16 oscillator frequency is plotted against dc supply voltage for a fixed grid bell length and cathode-short distance. From the curve it is apparent that there is very little change in frequency over a wide range of plate voltages, indicating a very low pushing figure.

In the system checkout under field conditions at CBA, 880 kw of pulse rf power was obtained from the oscillator at the 0.0015 duty with the frequency set at 218.9 Mc. For these tests the grid bell length was 11-1/2 inches and the cathode-short position was 21 inches as measured from the grid ring of the vacuum tube. Graduations are provided on the outer cylinder to set these grid bell and cathode-short distances. Pulse voltage was

[redacted]

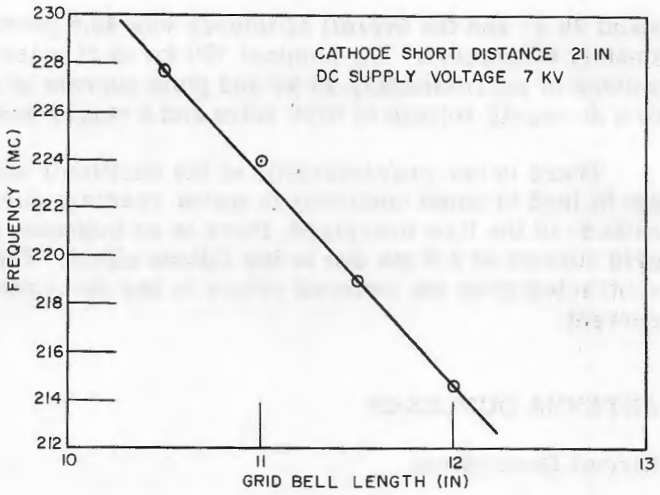

Fig. 14 - Oscillator frequency vs grid bell length for a constant cathode short-circuit position. To obtain this curve the double-stub tuner in the output coaxial line was adjusted for maximum power output as indicated on the power monitor for each point.

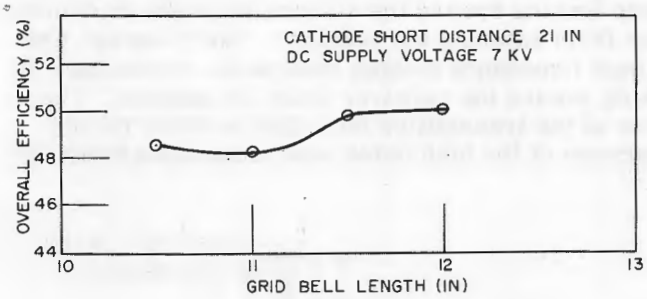

Fig. 15 - Overall efficiency vs grid bell length for a constant cathode short-circuit position. To obtain this curve the double-stub tuner in the output coaxial line was adjusted for maximum power output as indicated on the power monitor for each point.

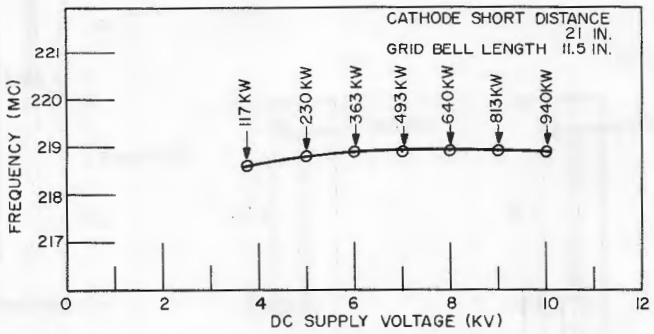

Fig. 16 - Oscillator frequency vs dc supply voltage for a constant grid bell length and cathode short-circuit position. To obtain this curve the double-stub tuner in the output coaxial line was adjusted for maximum power output as indicated on the power monitor for a dc supply voltage of 7 kv. This setting of the stub-tuner was kept throughout the test. The power noted at each voltage is the corresponding pulse rf output from the oscillator.

about 28 kv and the overall efficiency was 48.5 percent. Oscillator efficiency was approximately 60 percent. The nominal 750 kw of rf pulse power is obtainable at a pulse plate voltage of approximately 25 kv and plate current of around 50 amperes. This corresponds to a dc supply voltage of 8750 volts and a supply current of 265 ma.

There is one characteristic of the oscillator which should be pointed out, since it is apt to lead to some confusion in meter readings during normal operation. With only the cathode of the tube energized, there is an indicated plate current of 10 ma and an indicated grid current of 3.6 ma due to the Edison effect. These Edison currents should always be subtracted from the metered values in any determination of true average plate or grid current.

ANTENNA DUPLEXER

Circuit Description

The duplexer for this application is of the familiar branched-line type as illustrated in Fig. 17. The method of operation on "transmit" (the gap fired) is the presentation of a high impedance at the junctions of the TR, the ATR, and the auxiliary ATR with the main transmission line and a matched impedance looking toward the antenna from the transmitter. This condition prevents appreciable power from entering the receiver. On "receive" (the gap unfired) the arrangement provides a high impedance looking toward the transmitter at the junction with the TR and a match looking toward the receiver from the antenna. The auxiliary ATR provides additional isolation of the transmitter from the receiver during reception. This isolation is necessary because of the high noise level emanating from the

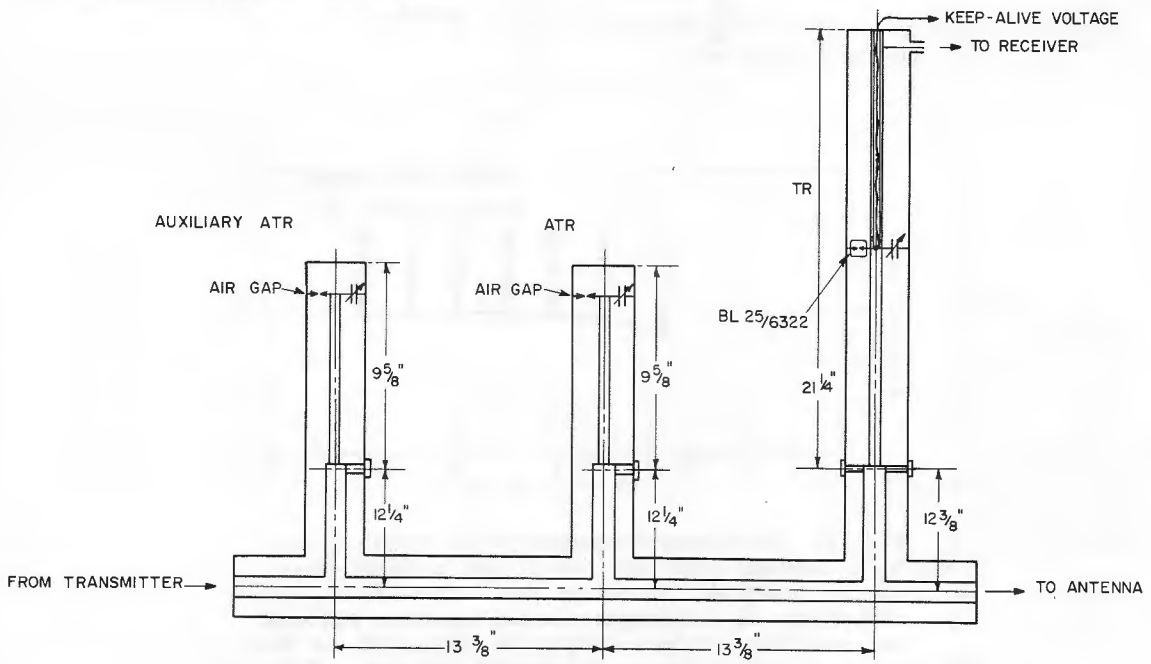

Fig. 17 - Branched coaxial duplexing system. The tanks are formed from 3-1/8-inch-diameter outer conductors, 1/2-inch-diameter inner conductors.

oscillator in the absence of rf power output. The noise is generated by the bombardment-type cathode. Air spark gaps are used for the ATR's and a BL-25/6322 is used for the TR switch. The keep-alive lead for the gas switch is brought in through the inner conductor of the TR tank.

Performance Characteristics

The duplexing system provides about 58 db protection for the receiver over the frequency range of the oscillator. While this has been found to be sufficient protection for the 416B tube used in the receiver rf amplifier, it may not be sufficient for the 6299 tube contemplated for use in the new receiver. If it is not, an auxiliary TR will be necessary. The insertion loss of an auxiliary TR is approximately 0.3 db.

The addition of the auxiliary ATR reduces the overall noise in the receiver by 6 db.

[redacted]

[redacted]

PART III - THE ANTENNAS

P. A. Lantz

ANTENNA REQUIREMENTS

A part of the 220-Mc radar development program was (a) the design and construction of a 14-element dipole array mounted on a 17-1/2 x 4 foot flat screen and (b) the design of a 56-element dipole array mounted on a 33-1/2 x 9 foot flat screen. It was originally contemplated that the 17-1/2 x 4 foot antenna would be mounted in an AN/APS-20C radome on a ZPG-2 airship. The 33-1/2 x 9 foot antenna design was to be provided to Goodyear Aircraft Corporation so that the antenna could be built into the gas envelope of a modified ZPG-2W airship under construction there. Plans for flying the 17-1/2-foot antenna were dropped after its construction was nearly complete, but the small antenna was convenient for use in ground tests of the system at CBA.

DESIGN OF THE 17-1/2-FOOT ANTENNA

Several basically different antenna types were considered for the specified 17-1/2 x 4 foot aperture, and it was decided that a two-dimensional array of dipoles offered the greatest advantages. This type of antenna gave the highest gain, and the side lobes were easily controlled. Moreover, the number of dipoles would not be excessive, since at half-wave spacing a 7 x 2 array of 14 dipoles would fill the aperture. It immediately became apparent that this represented the upper (or lower) half of a 220-Mc AN/SPS-17 antenna (18), manufacturing drawings of which were available.

The radiating elements chosen for this application were simple half-wave dipoles mounted on modified British-type coaxial baluns. The baluns consist of a length of standard 1-5/8-inch aluminum coaxial line with the outer conductor slit back a quarter wavelength and with an inner conductor of suitable size to match the dipole to a 51.5-ohm line. One side of the split outer conductor is shorted to one half of the dipole, and the entire assembly is wrapped with glass-cloth laminate to render it gas and water tight and give it mechanical rigidity. The radiators can be seen in Fig. 18, which is a photograph of the all-aluminum antenna. The dipole mounting gussets seen in the picture are glass-cloth laminate and are an integral part of the balun wrapper. The IFF antenna mounted at the top edge of the reflector is a standard AN/UPA-22 antenna. Figure 19 is a photograph of the back of the antenna showing the feed system, which is constructed of 1-5/8-inch aluminum coaxial line with a section of 3-1/8-inch coaxial line at the input.

A Dolph-Tschebyscheff horizontal current distribution was chosen to yield 31-db sidelobes, and Fig. 20 is the theoretical horizontal pattern that was expected from this array at 220 Mc. At half power, the theoretical beamwidth is 18.4 degrees. The currents were equally distributed in the vertical plane. Figure 21 is the calculated vertical pattern at 225 Mc, with a theoretical beamwidth of 51 degrees.

The input impedances of the dipoles, spaced $\lambda/8$ from the reflecting screen, were computed with the aid of Carter's formulas for the mutual impedance between rows of colinear dipoles (19). The results are summarized in Table 3. It should be recognized that the actual impedances of the dipoles depend on the current distribution as well as the mutual impedances.

[redacted]

Fig. 18 . Front view of the 17-1/2-foot antenna

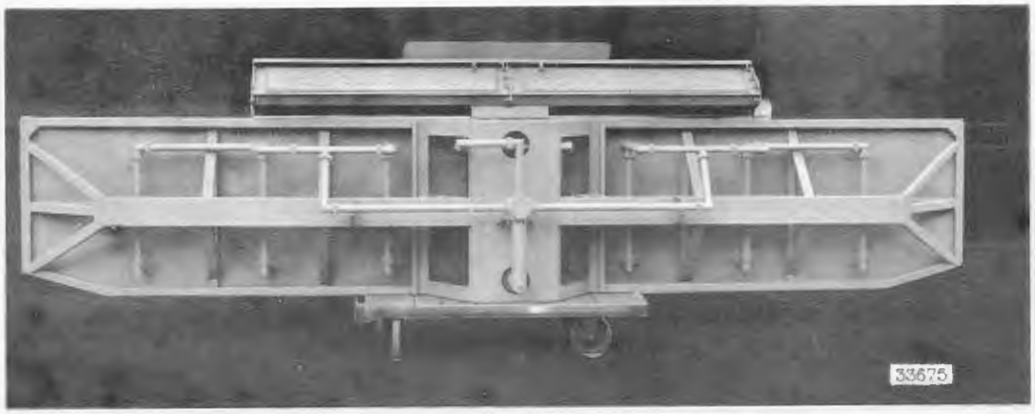

Fig. 19 - Rear view of the 17-1/2-foot antenna

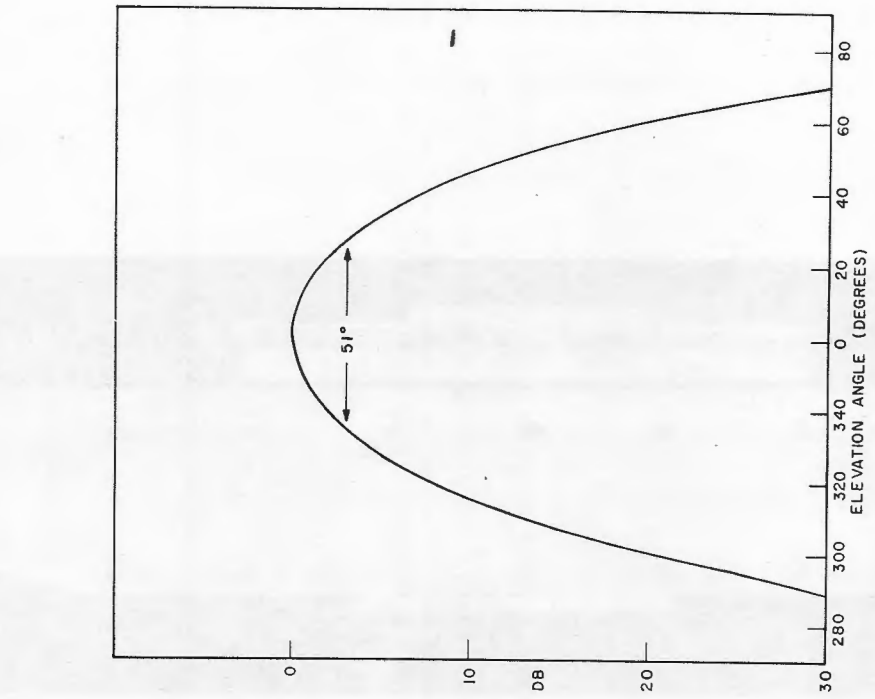

Fig. 21 - Theoretical H-plane pattern of the 17-1/2-foot antenna at 225 Mc

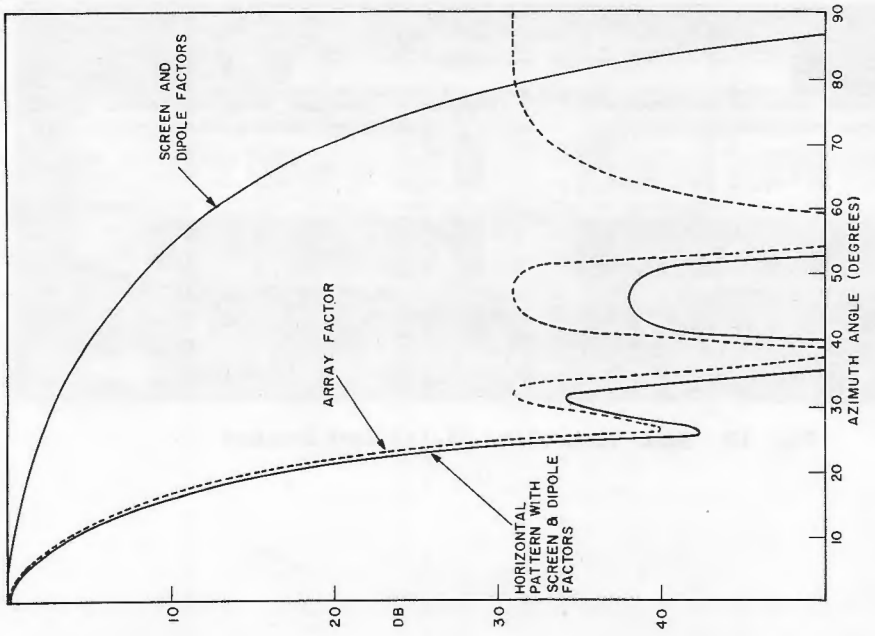

Fig. 20 - Theoretical E-plane pattern of the 17-1/2-foot antenna at 220 Mc

TABLE 3
Input Impedance of Half-Wave Dipoles Mounted at Half-Wave Intervals and Spaced $\lambda/8$ In Front of the Reflecting Sheet

Dipole Row-j	Dipole Column-i						
	1	2	3	4	5	6	7
1	$\frac{74.05}{j101.81}$	$\frac{72.47}{j109.49}$	$\frac{69.62}{j108.69}$	$\frac{69.03}{j108.58}$	$\frac{69.62}{j108.69}$	$\frac{72.47}{j109.49}$	$\frac{74.05}{j101.81}$
2	$\frac{74.05}{j101.81}$	$\frac{72.47}{j109.49}$	$\frac{69.62}{j108.69}$	$\frac{69.03}{j108.58}$	$\frac{69.62}{j108.69}$	$\frac{72.47}{j109.49}$	$\frac{74.05}{j101.81}$

The gain of the antenna was computed from the expression

$$G_{db} = 2.14 + 10 \log_4 \frac{(73.29)\left(2 \sin \frac{2\pi a}{\lambda}\right)^2 \left(\sum_{j=1}^{7} \sum_{j=1}^{2} I_{ij}\right)^2}{\sum_{j=1}^{7} \sum_{j=1}^{2} R_{ij} I_{ij}^2} \qquad (1)$$

in which 2.14 represents the gain of a half-wave dipole in free space and 73.29 its radiation resistance, a is the screen spacing and $2 \sin (2\pi a/\lambda)$ is the resultant field of a dipole and its image, and I_{ij} and R_{ij} are the current and input resistance of the dipole in the ith column and jth row. After substitution of these values we have

$$G_{db} = 2.14 + 10 \log \frac{(73.29)\ (1.4142)^2\ (8.72)^2}{447.448}$$

$$= 2.14 + 13.96 = 16.10 \text{ db.}$$

Figure 22 is a schematic diagram of the feed system. The baluns were built so that the impedance looking into each balun would be 51.5 ohms. Although some variation in dipole resistance is indicated in Table 3, the balun diameters were all made the same to simplify construction. This assumes an average dipole resistance of 70 ohms. In Fig. 22a the Dolph-Tschebyscheff current distribution for a sidelobe ratio of 31 db is shown. The relative power to be delivered to each of the balun-dipole assemblies has been computed by squaring the current ratios, on the assumption that the dipole resistances are equal. The power entering and leaving the junction points is indicated. In Fig. 22b these powers are normalized to a unity input power at each junction. Figure 22c shows the branch-point impedances required to effect the power divisions of Figs. 22a and 22b. In Fig. 22d the double quarter-wave transformers needed to match the feed system are given, and the corresponding inner conductor diameters to accomplish this are given in Fig. 22e. The feed system was built of aluminum coaxial line which had an outer conductor whose inner diameter was 3.027 inches in the 3-1/8-inch line, and 1.509 inches in the 1-5/8-inch line. Figure 22f indicates the potential gradients to be expected at several points throughout the feed system when the transmitter is delivering 1 megawatt. The maximum gradient of 15.5 kv/inch provides an ample safety factor.

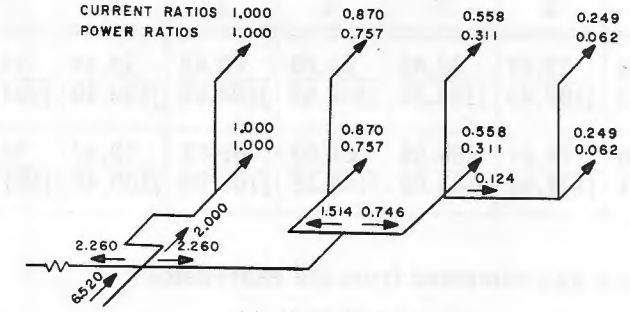

(A) POWER DISTRIBUTION

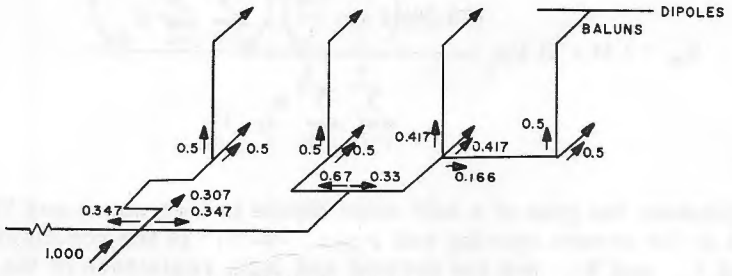

(B) NORMALIZED POWER DISTRIBUTION

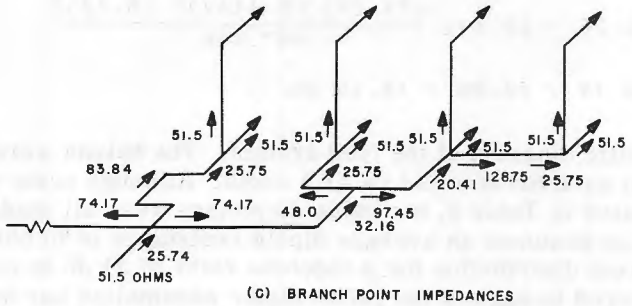

(C) BRANCH POINT IMPEDANCES

Fig. 22 - Feed system of the 17-1/2-foot antenna (cont'd)

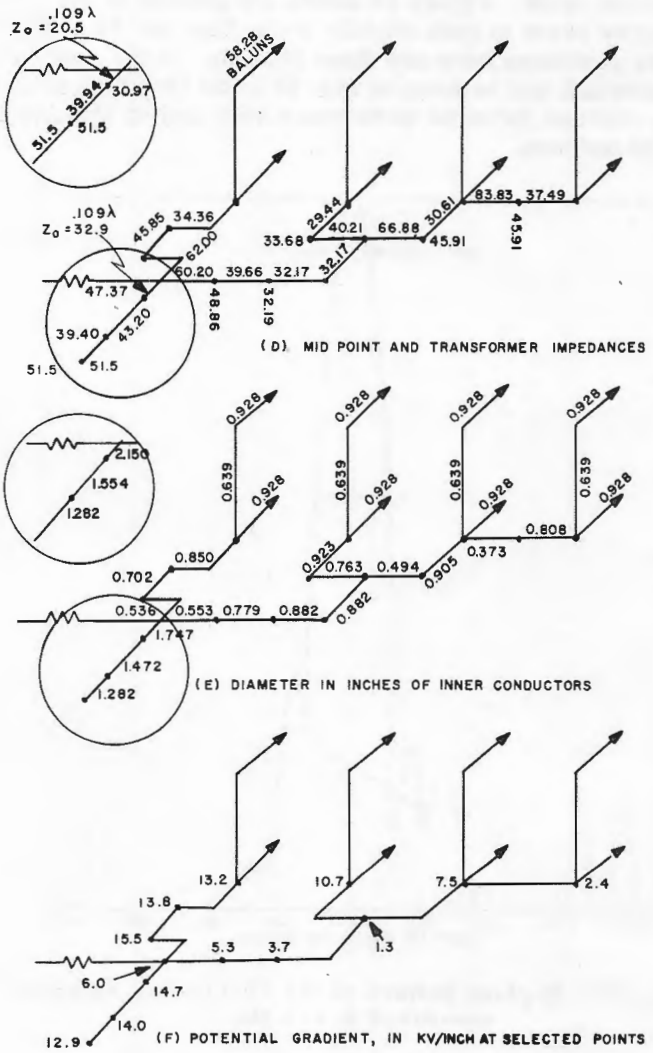

Fig. 22 - Feed system of the 17-1/2-foot antenna

PERFORMANCE OF THE 17-1/2-FOOT ANTENNA

The horizontal radiation patterns were measured on the 380-foot, low-frequency pattern range at CBA. In Fig. 23 the pattern at 216 Mc is shown. The half-power beamwidth was measured to be 19.3 degrees as indicated, and the sidelobes come up to 26.8 db, or about 4 db above the theoretical value. Figure 24 shows the pattern at the mid-band frequency of 220 Mc. The 18.8-degree beam is only slightly wider than the 18.4-degree theoretical width (Fig. 20), and the sidelobes here are down 29.4 db. At the upper end of the frequency band (225 Mc) the beamwidth can be seen in Fig. 25 to be 18.4 degrees, and the sidelobes are down 28.4 db. No vertical patterns were measured, and no attempt was made to measure the gain of the antenna.

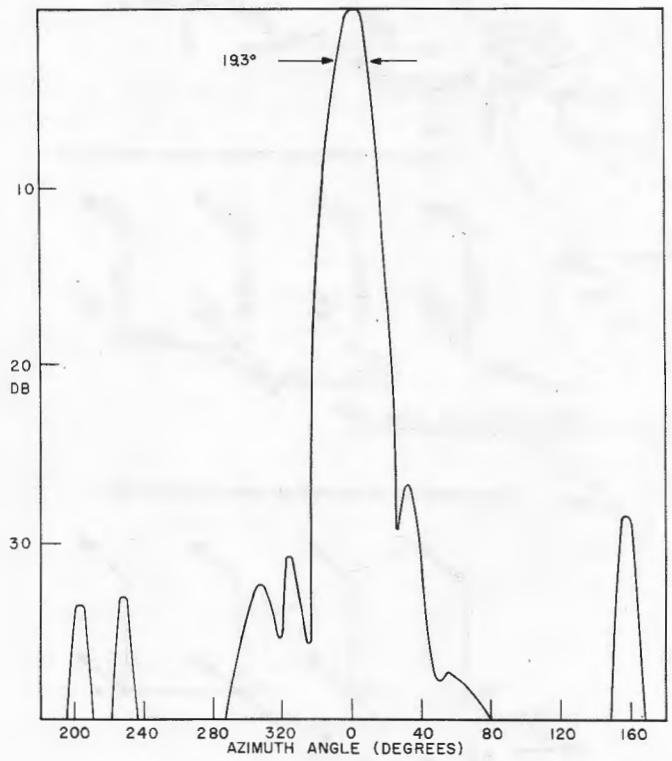

Fig. 23 - E-plane pattern of the 17-1/2-foot antenna measured at 216 Mc

A matching section was built in the 3-1/8-inch input coaxial line as shown in Fig. 22d. Since the antenna was slightly reactive, the 0.109λ length of 32.9-ohm line was used with a 43.2-ohm quarter-wave transformer to match to a 51.5-ohm input. The input terminal impedance with this arrangement is shown as curve A on Fig. 26. Although the input voltage standing-wave ratio ranged from 1.4 to 1.5 over the band 216-225 Mc, the transmitter worked satisfactorily into the antenna load during the system testing. It has been determined that a better input impedance could be achieved if the input coaxial sections were rebuilt as shown in the inset circles on Figs. 22d and 22c. The expected impedance is plotted as curve B in Fig. 26 and the theoretical VSWR over the band would then be less than 1.35.

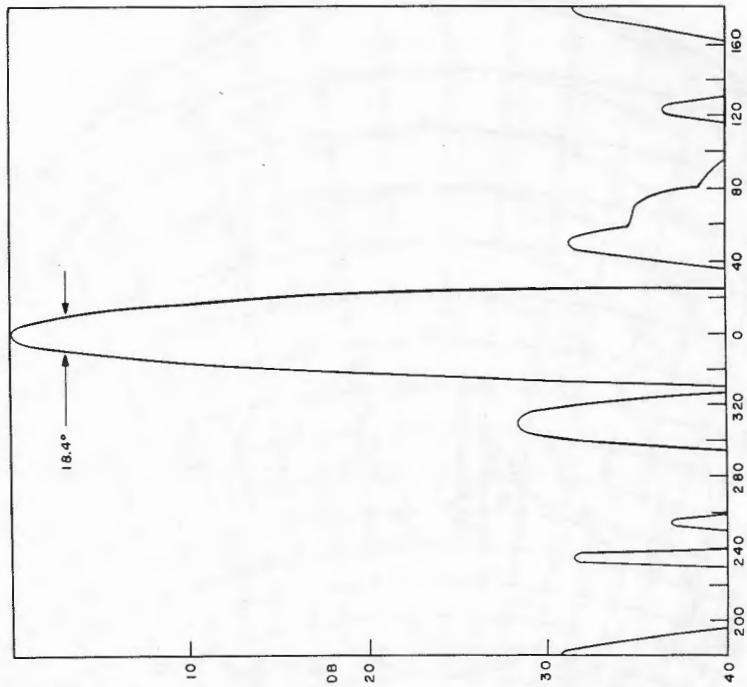

Fig. 25 - E-plane pattern of the 17-1/2-foot antenna measured at 225 Mc

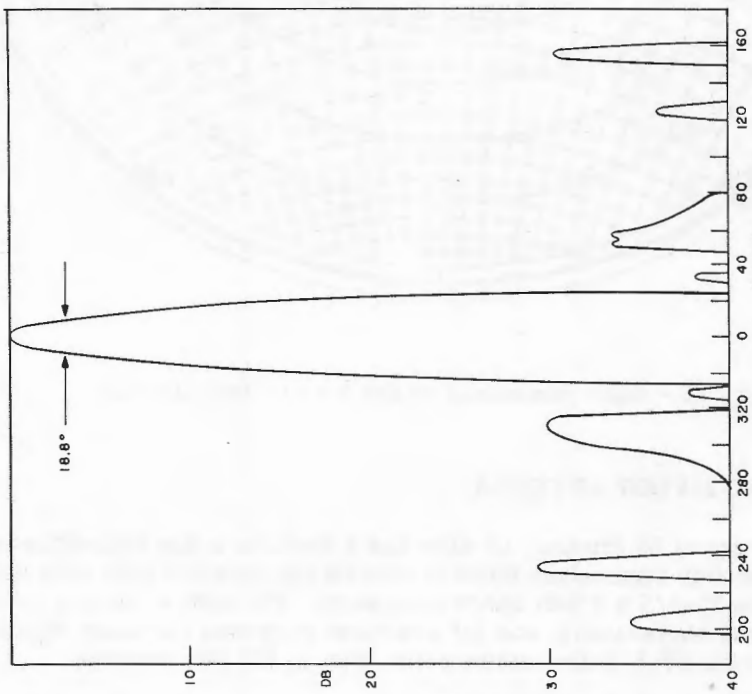

Fig. 24 - E-plane pattern of the 17-1/2-foot antenna measured at 220 Mc

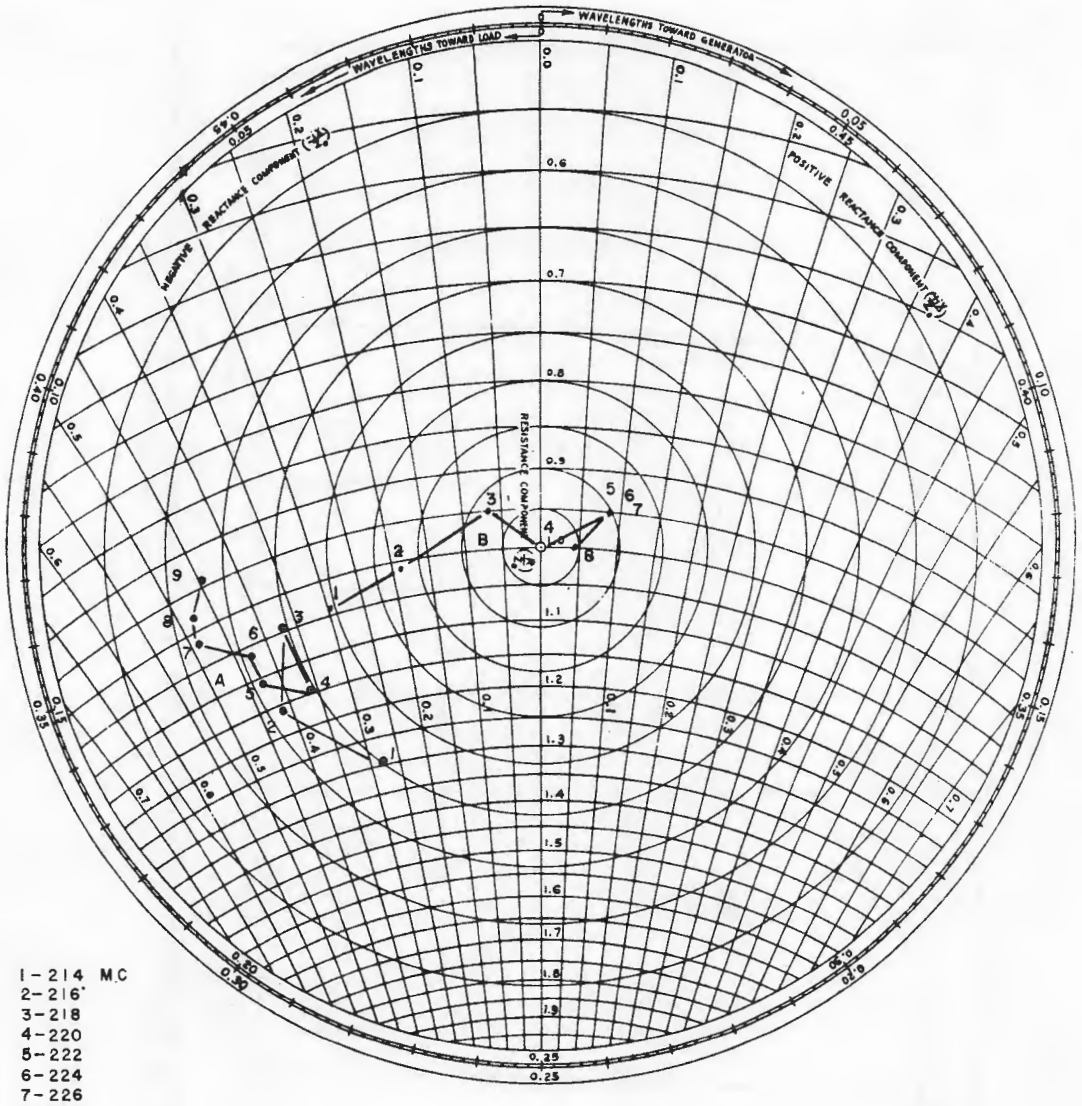

Fig. 26 - Input impedance of the 17-1/2-foot antenna

DESIGN OF THE 33-1/2-FOOT ANTENNA

The use of an array of 56 dipoles, 14 wide and 4 high, on a flat reflecting screen, was arbitrarily chosen for this application since it offered the greatest gain with minimum side-lobes, considering the 33-1/2 x 9 foot space limitation. The dipole spacing was set to be $\lambda/2$ both vertically and horizontally, and for practical purposes the same dipole-balun arrangement used on the 17-1/2-foot antenna was chosen for this antenna.

An experiment was set up to determine the best dipole diameter and screen spacing in terms of antenna bandwidth. It was found that there was very little improvement in bandwidth when the dipole diameter was increased from 5/8 inch to 1-1/4 inches. The

smaller diameter was chosen because it has less end-to-end capacitance and weighs less. Figure 27 shows the effect of varying the spacing between the dipole and the reflecting screen. In conducting this experiment, a single dipole in front of a flat screen was used. The dipole was resonated at each screen spacing and a length of RG-8/U, cut to be $\lambda/2$ at 220 Mc, connecting an impedance bridge to the balun, was corrected at each frequency so that all measurements were referred to the back of the balun. It can be seen that the greatest bandwidth was obtained when this space was adjusted so s/λ was 0.168 or 9 inches, and that at this setting the VSWR did not exceed 1.3 over the band 216.5 to 225 Mc. Although a somewhat lower VSWR could have been obtained with a folded dipole, the 1.3 value was considered to be acceptable and, therefore, the straight dipole, which is mechanically simpler, was chosen.

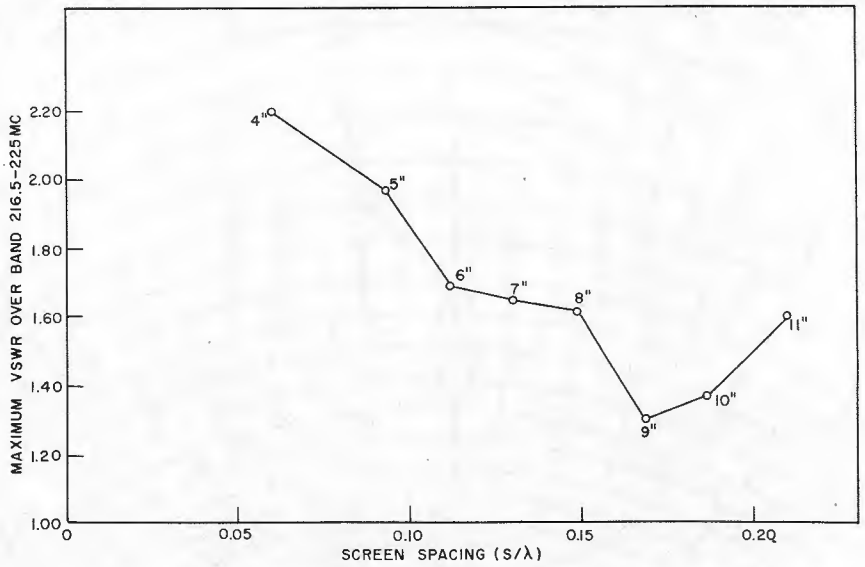

Fig. 27 - Effect of varying the dipole screen spacing on the 33-1/2-foot antenna

Since the British-type slotted balun (20,21) worked satisfactorily on the 17-1/2-foot antenna, it was selected for use with the larger antenna. Experiments were conducted, however, to determine the optimum slot length and width and to determine the effect of wrapping the slot with glass-cloth laminate. With the dipole adjusted for resonance at 220 Mc, the slot length and width of an unwrapped balun were adjusted and the resultant change in impedance was observed.

It was found that the impedance was more sensitive to variations in slot length than to changes in slot width. Moreover, lengthening the slot beyond $\lambda/4$ increased the resistive component and made the reactance more negative (i.e., capacitive). The main effect of changing the slot width was to vary the rate at which the reactance changed. When the slot was too narrow it was difficult to resonate the dipole. When the slot was too wide, the magnitude of the reactance became very large at the ends of the band 216.5 to 220 Mc.

In addition, it was found that wrapping the balun with glass-cloth laminate affected only the length of the slot, making it appear slightly greater than its physical length. The optimum slot width was determined to be 0.250 inch in the standard 1-5/8-inch coaxial line

used, and the optimum slot length of the unwrapped balun was found to be 0.223λ. When the balun was wrapped, the optimum slot length became 0.209λ. Figure 28 is a plot of the impedance of the balun and dipole combination which was used on the antenna.

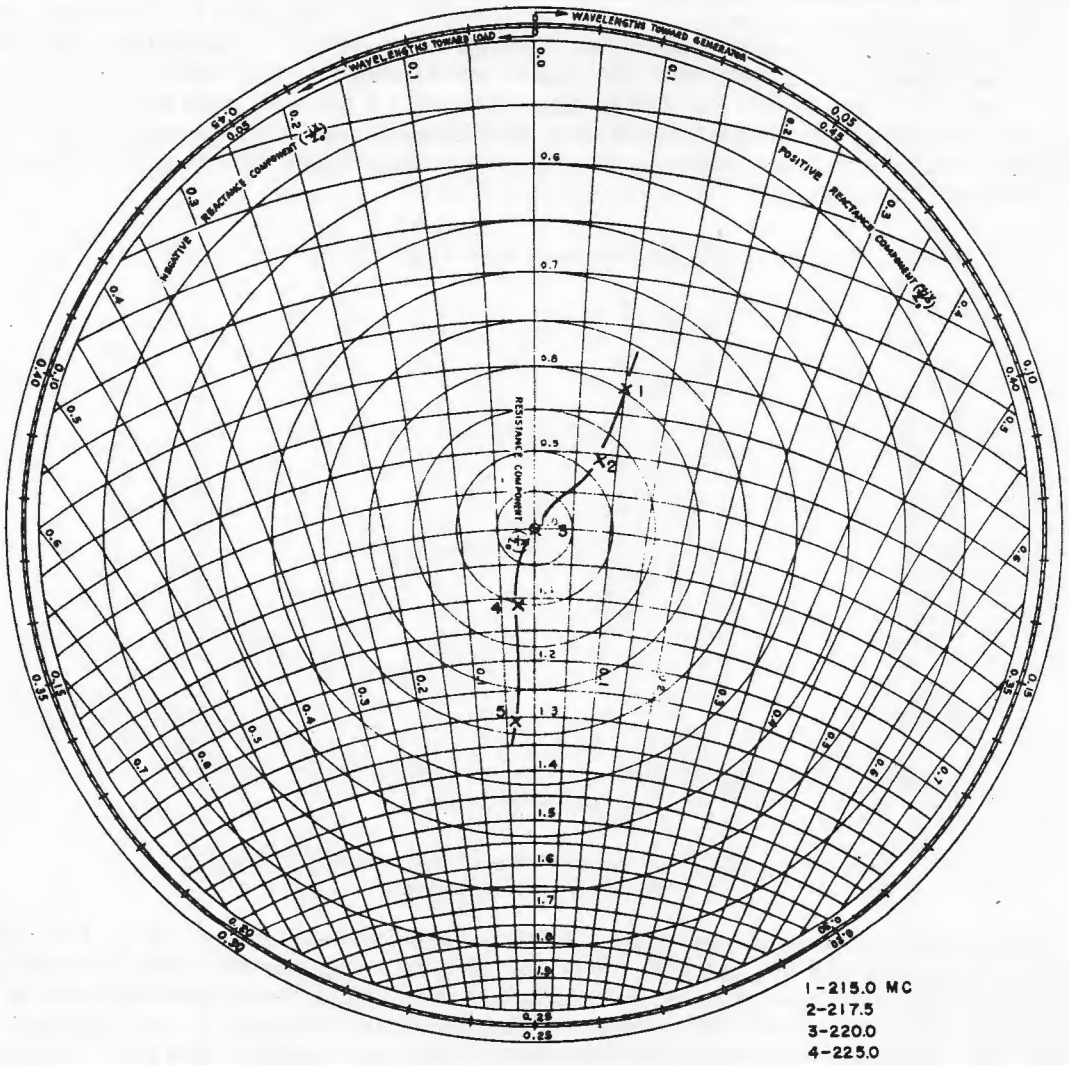

Fig. 28 - Impedance of a single dipole as used on the 33-1/2-foot antenna

A horizontal current distribution of 1.00, 0.94, 0.84, 0.70, 0.54, 0.38, and 0.34 was chosen based on a Dolph-Tschebyscheff distribution for a sidelobe ratio of 28 db. The theoretical pattern to be expected from this distribution is shown in Fig. 29, and the computed beamwidth is 8.92 degrees as indicated. A vertical current distribution of 0.724, 1.000, 1.000, and 0.724 was arbitrarily chosen in preference to a uniform current distribution, making possible a theoretical reduction of the sidelobe level from 14 db to 18.6 db. The current distribution among the dipoles is shown in Table 4. The vertical pattern was checked by constructing a section of the antenna consisting of one column of dipoles and measuring the resultant pattern. The patterns measured at 216, 220, and 225 Mc are shown in Fig. 30, where the mid-band beamwidth can be seen to be 30 degrees and the sidelobe level 16.6db.

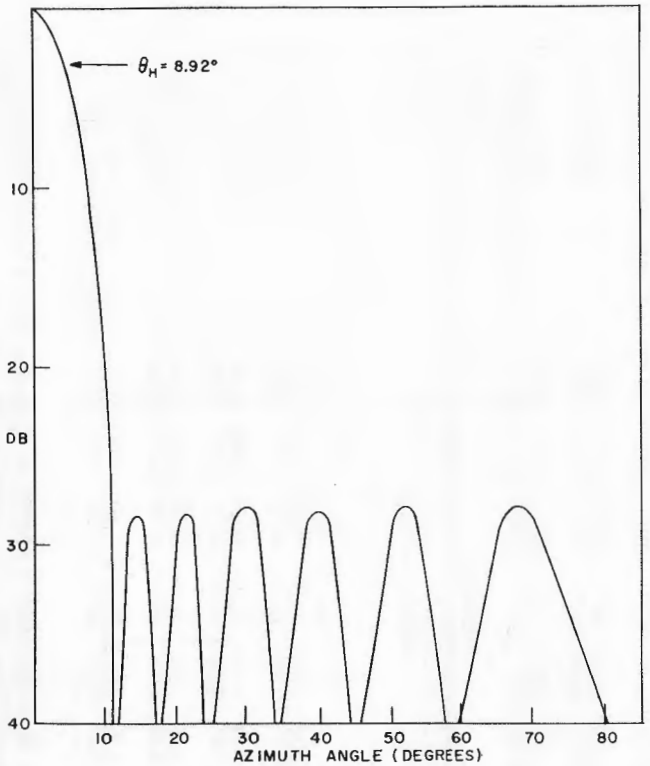

Fig. 29 - Theoretical E-plane pattern of the 33-1/2-foot antenna at 220 Mc

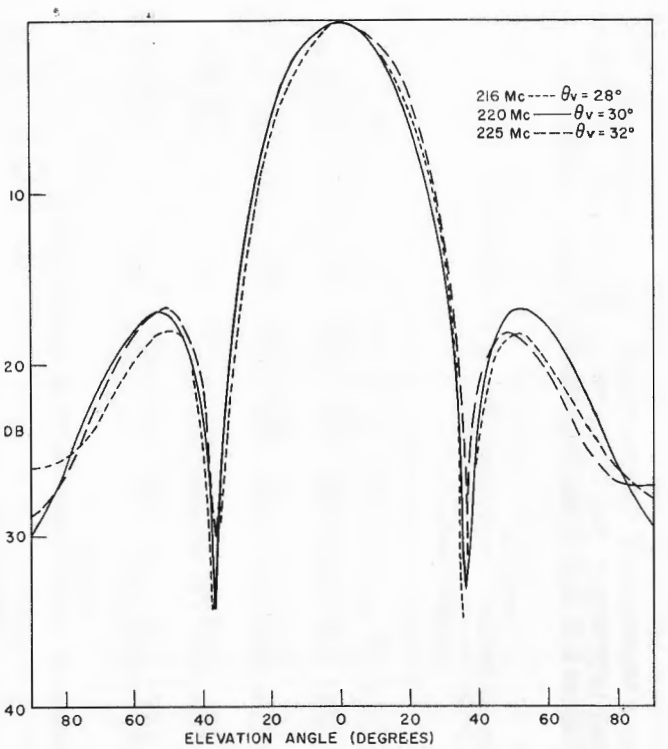

Fig. 30 - H-plane patterns measured on the vertical section of the 33-1/2-foot antenna

TABLE 4
Distributions of Currents Among the Dipoles of the 33-1/2-Ft Antenna

Dipole Row-j	Dipole Column-i													
	1	2	3	4	5	6	7	8	9	10	11	12	13	14
1	0.2451	0.2722	0.3891	0.5059	0.6086	0.6843	0.7240	0.7240	0.6843	0.6086	0.5059	0.3891	0.2722	0.2451
2	0.3385	0.3765	0.5374	0.6987	0.8406	0.9451	1.0	1.0	0.9451	0.8406	0.6987	0.5374	0.3765	0.3385
3	0.3385	0.3765	0.5374	0.6987	0.8406	0.9451	1.0	1.0	0.9451	0.8406	0.6987	0.5374	0.3765	0.3385
4	0.2451	0.2722	0.3891	0.5059	0.6086	0.6843	0.7240	0.7240	0.6843	0.6086	0.5059	0.3891	0.2722	0.2451

In order to design the feed system (power divider) of the antenna, an extensive mathematical computation was performed to determine the theoretical dipole impedances. The method used for calculating mutual impedances was that given by Carter (19). The resultant dipole impedances are given in Tables 5, 6, and 7, and the effective dipole impedances are summarized in Table 8.

TABLE 5
Calculated Mutual Impedances Between the Actual Dipoles of the 33-1/2-Ft Antenna

Dipole Row -j	Dipole Column -i													
	1	2	3	4	5	6	7	8	9	10	11	12	13	14
1	73.2 j42.5	26.49 j20.6	-3.95 -j0.72	1.80 -j0.195	-1.03 j0.075	0.525 j0.045	-0.713 j0.495	-0.375 j1.02	-0.450 j0.78	0.615 j0.51	0.090 -j0.48	-0.19 -j0.29	-0.285 j0.27	0.360 j0.18
2	-12.51 -j29.97	-11.91 -j7.86	-0.765 j2.58	0.870 -j4.35	-1.13 -j0.735	0.015 -j0.165	-1.185 j0.855	-0.840 j0.99	-0.885 j0.93	0.345 j0.255	-0.030 -j0.24	-0.255 -j0.225	-0.180 j0.30	0.405 j0.15
3	3.84 j17.91	8.85 j9.06	3.92 -j4.19	-2.73 -j0.345	1.05 j1.005	-0.510 -j0.48	0.036 j0.735	-0.393 -j0.225	-0.384 j0.645	0.390 -j0.075	-0.165 -j0.36	-0.225 -j0.435	-0.270 j0.405	0.165 j0.12
4	-1.89 -j12.33	-5.86 -j8.64	-6.30 j1.68	2.03 j3.00	0.555 -j2.07	-0.990 j0.84	0.960 -j0.51	-0.770 -j0.525	0.090 j0.42	0.090 -j0.225	0.480 -j0.045	0.360 -j0.405	-0.18 j0.39	0.225 j0.135

TABLE 6
Calculated Mutual Impedances Between the Dipole Images of the 33-1/2-Ft Antenna

Dipole Row -j	Dipole Column -i													
	1	2	3	4	5	6	7	8	9	10	11	12	13	14
1	21.0 -j36.8	1.54 -j14.9	-3.20 j2.24	1.59 -j0.64	-2.01 j0.25	0.57 -j0.12	-0.58 j0.108	0.12 -j0.030	-0.27 j0.03	0.383 -j0.045	0.144 -j0.015	0.345 -j0.095	0.108 -j0.015	0.17 j0
2	-23.42 -j16.6	-14.1 j0.54	1.51 j4.16	0.48 -j1.87	-0.44 j0.80	0.47 -j0.49	-0.31 j0.27	0.26 -j0.19	-0.28 j0.11	0.18 -j0.075	-0.018 j0.075	0.30 -j0.06	-0.045 j0.03	-0.013 j0
3	9.11 j14.73	11.13 j5.51	3.39 -j4.93	-1.66 j1.06	1.90 j0.97	-0.56 -j0.70	-0.04 j0.55	-0.07 -j0.39	-0.007 j0.27	0.04 -j0.22	-0.06 j0.20	0.04 -j0.12	-0.13 j0.14	-0.10 -j0.01
4	-4.48 -j11.31	-7.42 -j7.95	-5.74 j3.08	2.61 j2.71	0.26 -j2.20	-0.99 j0.95	0.82 -j0.34	-0.61 -j0.02	0.41 j0.11	-0.38 -j0.16	0.18 j0.18	-0.11 -j0.17	0.08 j0.12	-0.016 -j0.12

TABLE 7
Calculated Sum of Mutual Impedances Between Dipoles and Images of the 33-1/2-Ft Antenna

Dipole Row -j	Dipole Column -i													
	1	2	3	4	5	6	7	8	9	10	11	12	13	14
1	52.2 j79.3	24.95 j35.06	-0.75 -j2.96	0.21 j0.445	0.98 -j0.175	-0.045 j0.165	-0.133 j0.387	-0.495 j1.05	-0.18 j0.75	0.232 j0.555	-0.135 -j0.465	-0.535 -j0.255	-0.393 j0.285	0.19 j0.18
2	10.91 -j13.37	2.19 -j8.4	-2.27 -j1.58	0.39 -j2.48	-0.69 -j1.535	-0.455 j0.325	-0.875 j0.585	-1.1 j1.18	-0.605 j0.82	0.165 j0.330	-0.012 -j0.315	-0.555 -j0.219	0.135 j0.27	0.418 j0.15
3	-5.27 j3.18	-2.28 j3.55	0.53 j0.74	-1.07 -j1.405	-0.85 j0.035	0.05 j0.22	0.076 j0.185	-0.386 j0.165	-0.377 j0.375	0.350 j0.145	0.171 j0.56	-0.229 -j0.423	-0.14 j0.265	0.265 j0.13
4	2.59 -j1.02	1.56 -j0.69	-0.56 -j1.4	-0.58 j0.29	0.295 j0.13	0 -j0.11	0.14 -j0.17	-0.16 -j0.505	-0.32 j0.31	0.47 j0.385	0.30 -j0.225	0.47 -j0.235	-0.26 j0.27	0.241 j0.255

A schematic diagram of the feed system is shown in Fig. 31 where the terminus of each quarter-wave transformer is shown by a dot. Only one of the fourteen identical vertical columns is shown. A primary consideration in the layout of the system was the fact that it can be shown that the current distribution to the dipoles is unaffected by the individual dipole impedances when each dipole is an odd quarter-wave length away from all points

TABLE 8
Calculated Effective Dipole Impedances of the 33-1/2-Ft Antenna

Dipole Row -j	Dipole Column -i													
	1	2	3	4	5	6	7	8	9	10	11	12	13	14
1	65.76 j92.2	97.07 j130.66	96.36 j105.8	99.71 j102.94	100.43 j102.67	101.11 j101.62	101.97 j100.82	101.97 j100.82	101.11 j101.62	100.43 j102.67	99.71 j102.94	96.36 j105.8	97.07 j130.66	65.76 j92.2
2	69.22 j86.89	102.92 j105.08	101.39 j89.97	105.12 j89.27	107.05 j87.99	107.96 j87.16	108.18 j86.45	108.18 j86.45	107.96 j87.16	107.05 j87.99	105.12 j89.27	101.39 j89.97	102.92 j105.08	69.22 j86.89
3	69.22 j86.89	102.92 j105.08	101.39 j89.97	105.12 j89.27	107.05 j87.99	107.96 j87.16	108.18 j86.45	108.18 j86.45	107.96 j87.16	107.05 j87.99	105.12 j89.27	101.39 j89.97	102.92 j105.08	69.22 j86.89
4	65.76 j92.2	97.07 j130.66	96.36 j105.8	99.71 j102.94	100.43 j102.67	101.11 j101.62	101.97 j100.82	101.97 j100.82	101.11 j101.62	100.43 j102.67	99.71 j102.94	96.36 j105.8	97.07 j130.66	65.76 j92.2

of power division between the dipole and the main feed point. Another consideration was the desirability of having the line lengths from the main feed point to all dipoles equal in order to preserve the phase of the currents at the dipoles.

In Fig. 31a, the relative power delivered to each dipole is obtained by squaring the dipole current on the assumption that the dipole resistances are all equal. The power entering and leaving the junction points is indicated. The branch-point impedances are shown in Fig. 31b, where it can be seen that the impedances at the junctions between the horizontal and vertical power dividers were all set to equal 51.5 ohms and the input terminal impedance was set to be 50.0 ohms. The midpoint and transformer impedances calculated to match the assumed 103-ohm dipoles to a 50-ohm input are given in Fig. 31c, and the required diameter ratios to effect the impedances are given in Fig. 31d.

Assuming the use of standard RTMA 1-5/8-inch rigid coaxial line in the power divider and standard RTMA 3-1/8-inch rigid coaxial line for the main feed line, voltage gradients were calculated at the inner conductor for critical points in the feed system. It was found that the maximum gradient occuring in the feed system was 15.5 kv/in., which is well below the theoretical 75-kv/in. breakdown point.

A nine-element array consisting of three rows of three dipoles each, was built to experimentally check the theoretical effective dipole impedances and resonant lengths. By changing the inner conductors, relative current distributions of each of the six possible groups of nine adjacent dipoles in the 56-element array could be duplicated. Effective dipole impedances and resonant lengths for all nine-element groups were then calculated and two representative groups were measured, one having the relative currents occurring in the center section of the 56-element array, and the other having the relative currents occurring at the extreme ends of the array. It was found that the measured effective impedances averaged within 10 percent of the calculated values. Figure 32 shows calculated and measured lengths and impedances for the center section of dipoles (i.e., columns 7, 8, and 9 counting from left to right facing the antenna). This is considered to be reasonable in consideration of the slotted-line measuring techniques employed, and the small standing-wave ratios encountered. The measured dipole resonant lengths averaged 5 percent greater than the theoretical* values (Fig. 32). This is attributed to the effect of mutual end capacitances.

*From transmission line theory it can be shown that the calculated effective dipole impedance is $Z_{input} = Z_o [-j (\coth \alpha\ell + \cot \beta\ell)/(\coth \alpha\ell)]$ and dropping the relatively small terms as shown $Z_{input} = -jZ_o \cot \beta\ell$ where $\beta = 2\pi/\lambda = 360/53.65$. The dipole lengths ($\ell$) were thereby computed from theoretical dipole impedance.

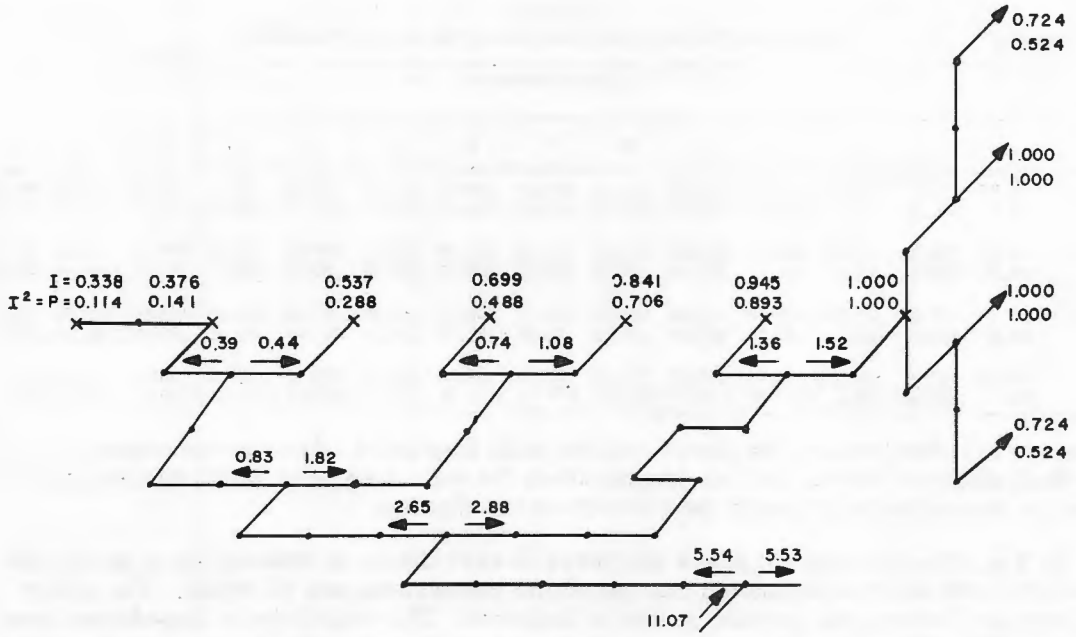

(A) POWER DISTRIBUTION

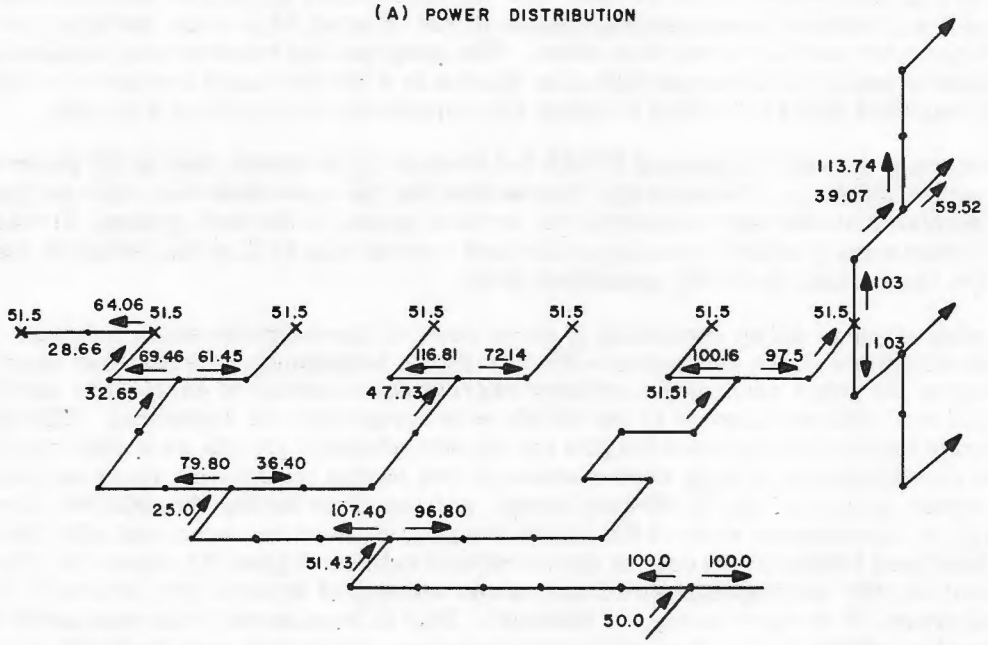

(B) BRANCH POINT IMPEDANCES

Fig. 31 - Feed system of the 33-1/2-foot antenna (cont'd)

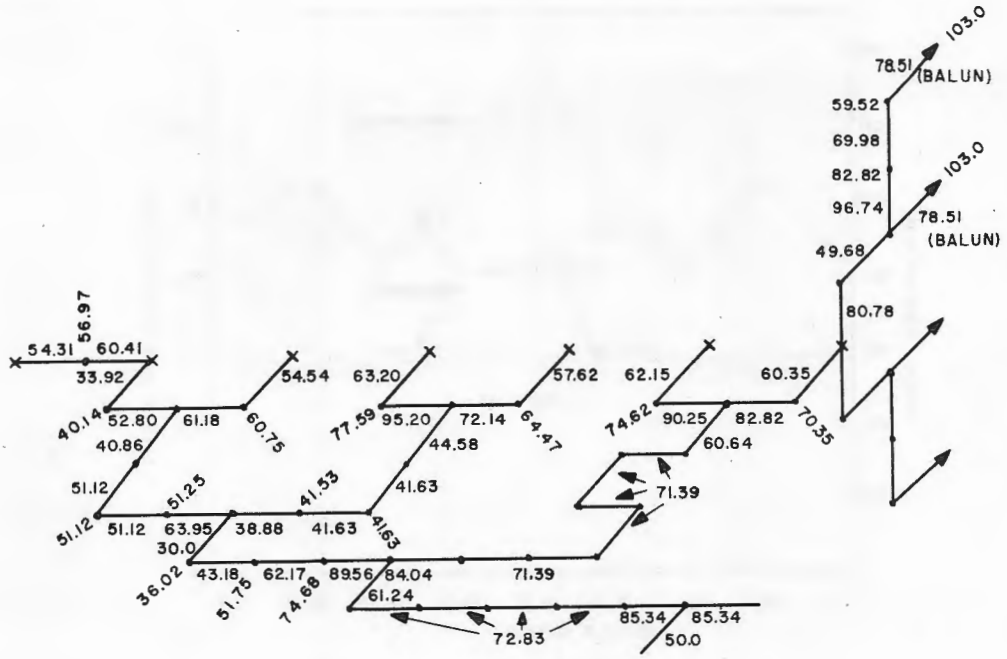

(C) MIDPOINT AND TRANSFORM IMPEDANCES

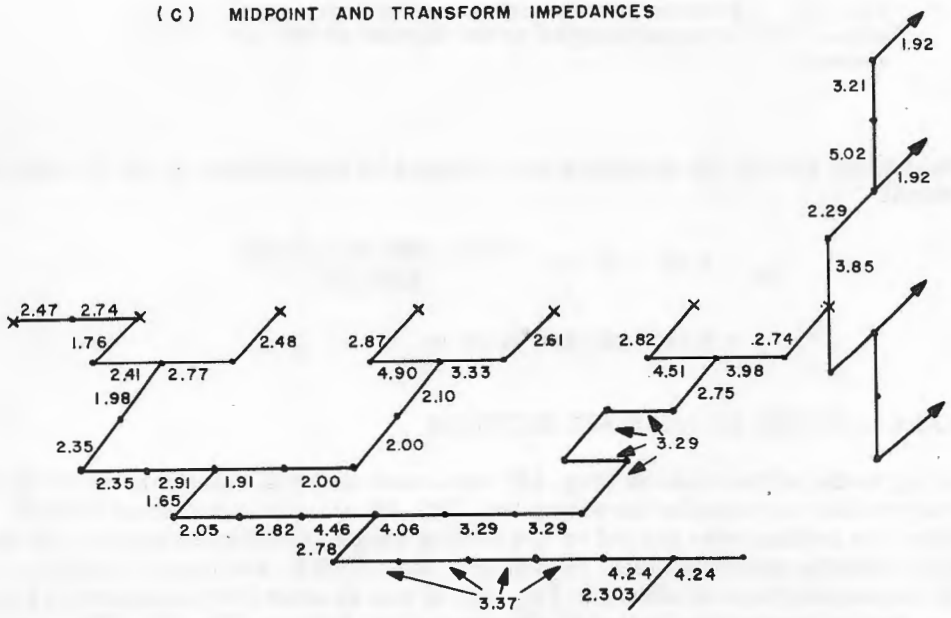

(D) RATIOS OF I.D. OUTER CONDUCTOR TO O.D. INNER CONDUCTOR

Fig. 31 - Feed system of the 33-1/2-foot antenna

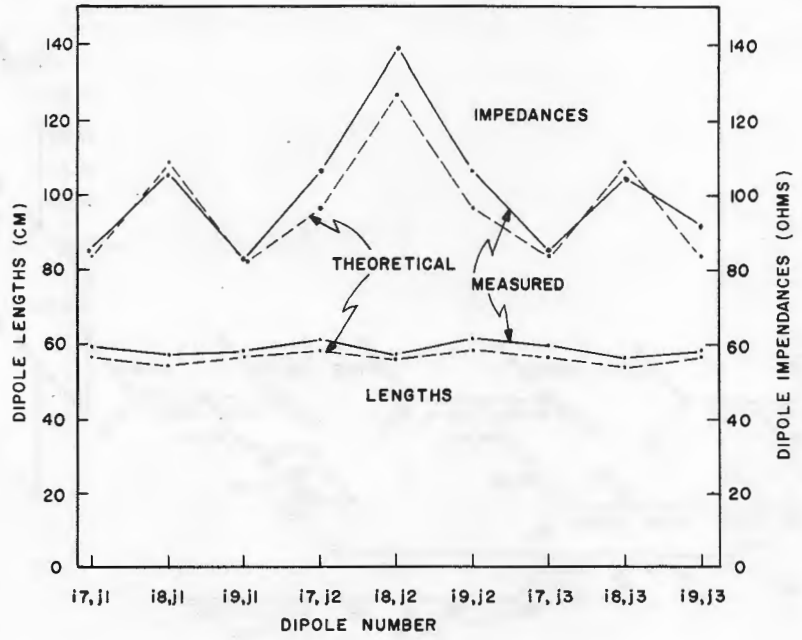

Fig. 32 - Agreement of the calculated and measured impedances and resonant lengths of the dipoles of the 33-1/2-foot antenna

The theoretical gain of the antenna was computed by substitution in Eq. (1) with the following result:

$$G_{db} = 2.14 + 10 \log \frac{73.29\ (1066.94)\ (3.024)}{2290.552}$$

$$= 2.14 + 20.14 = 22.28 \text{ db.}$$

PERFORMANCE OF THE 33-1/2-FOOT ANTENNA

A working model of the antenna (Fig. 33) was constructed in aluminum by the Goodyear Aircraft Corporation for installation within the ZPG-2W airship under construction. Prior to installation, the antenna was placed on the testing range at that company for the purpose of measuring radiation patterns, gain, impedance, input VSWR, and power-handling capability. The E-plane patterns are shown in Fig. 34. It can be seen that the measured beamwidths are in good agreement with that of the theoretical pattern (Fig. 29). The magnitude of the sidelobes could not be measured due to a limited dynamic range of received signal above noise. The H-plane patterns are shown in Fig. 35, where the beamwidths and sidelobes can be seen to compare favorably with the theoretical patterns shown in Fig. 30. Table 9 compares theoretical and measured performance.

The gain over an isotropic source was measured by calibrating a corner-reflector antenna by means of various methods and using it as a standard for comparison. The results are given in Table 10.

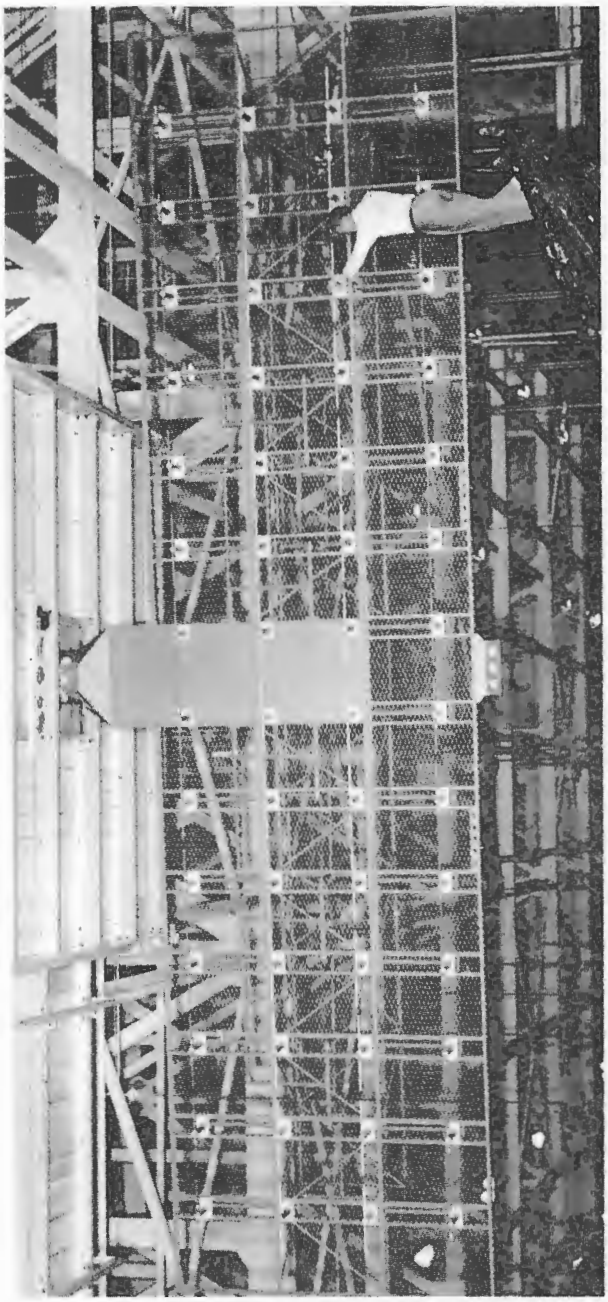

Fig. 33 - Front view of the 33-1/2-foot antenna

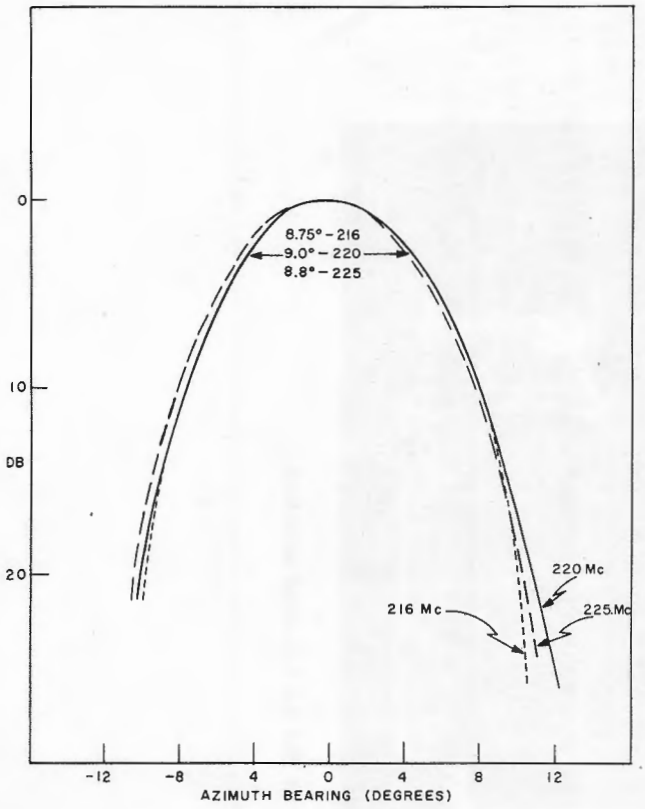

Fig. 34 - E-plane radiation patterns measured on the 33-1/2-foot antenna

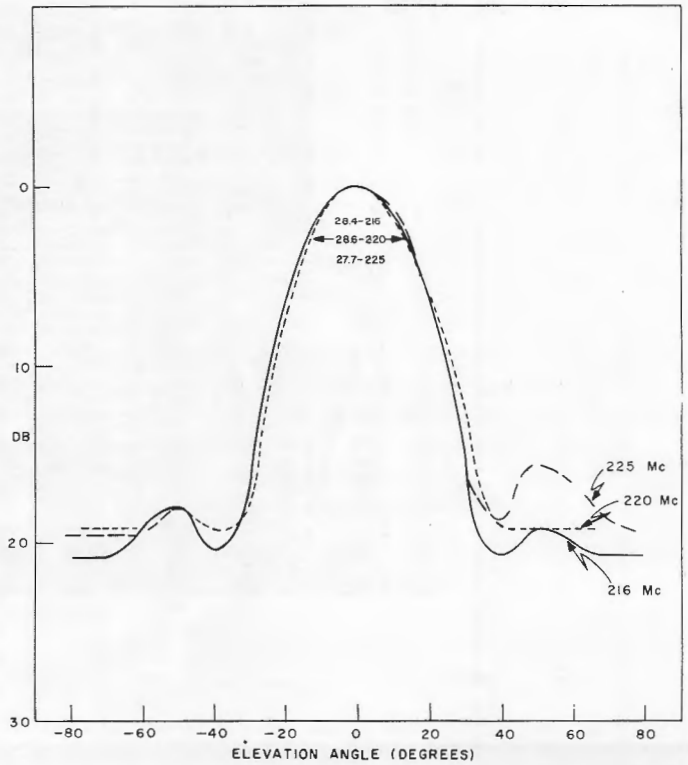

Fig. 35 - H-plane radiation patterns measured on the 33-1/2-foot antenna

TABLE 9
Comparison of Measured and Theoretical
Vertical Radiation Patterns

Frequency (Mc)	Beamwidth (degrees)		Max Sidelobe Level (db)	
	Theor.	Meas.	Theor.	Meas.
216	28	28.4	18.0	18.0
220	30	28.6	16.6	18.0
225	32	27.7	16.8	15.9

Since the gain, at mid-band, computed from the measured beamwidths would be

$$\frac{41,000}{\theta_v \times \theta_h} = \frac{41,000}{28.6 \times 9.0} = 159 \text{ or } 22.0 \text{ db}$$

it is considered that the measured values of gain may be in error, possibly as a result of inaccuracy in calibrating the comparison standards. This assumption is further borne out by the fact that the theoretical gain computed from Eq. (1) indicated the gain to be 22.3 db.

TABLE 10
Gain Over an Isotropic Source

Frequency (Mc)	Gain (db)
216	20.3
220	20.2
225	20.5

The input standing-wave ratio, plotted in Fig. 36, is constant at about 1.25 over the band 215 to 225 Mc. The input impedance, referred to the first T-junction, is shown in Fig. 37. Evidently the match could be improved in the 215 to 225 Mc band by the use of a suitable matching transformer.

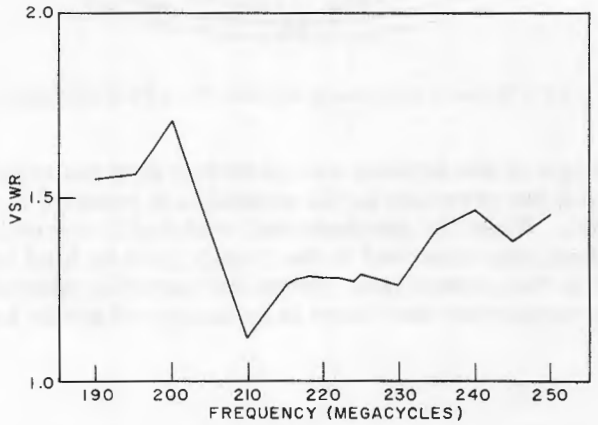

Fig. 36 - Input voltage standing-wave ratio of the 33-1/2-foot antenna

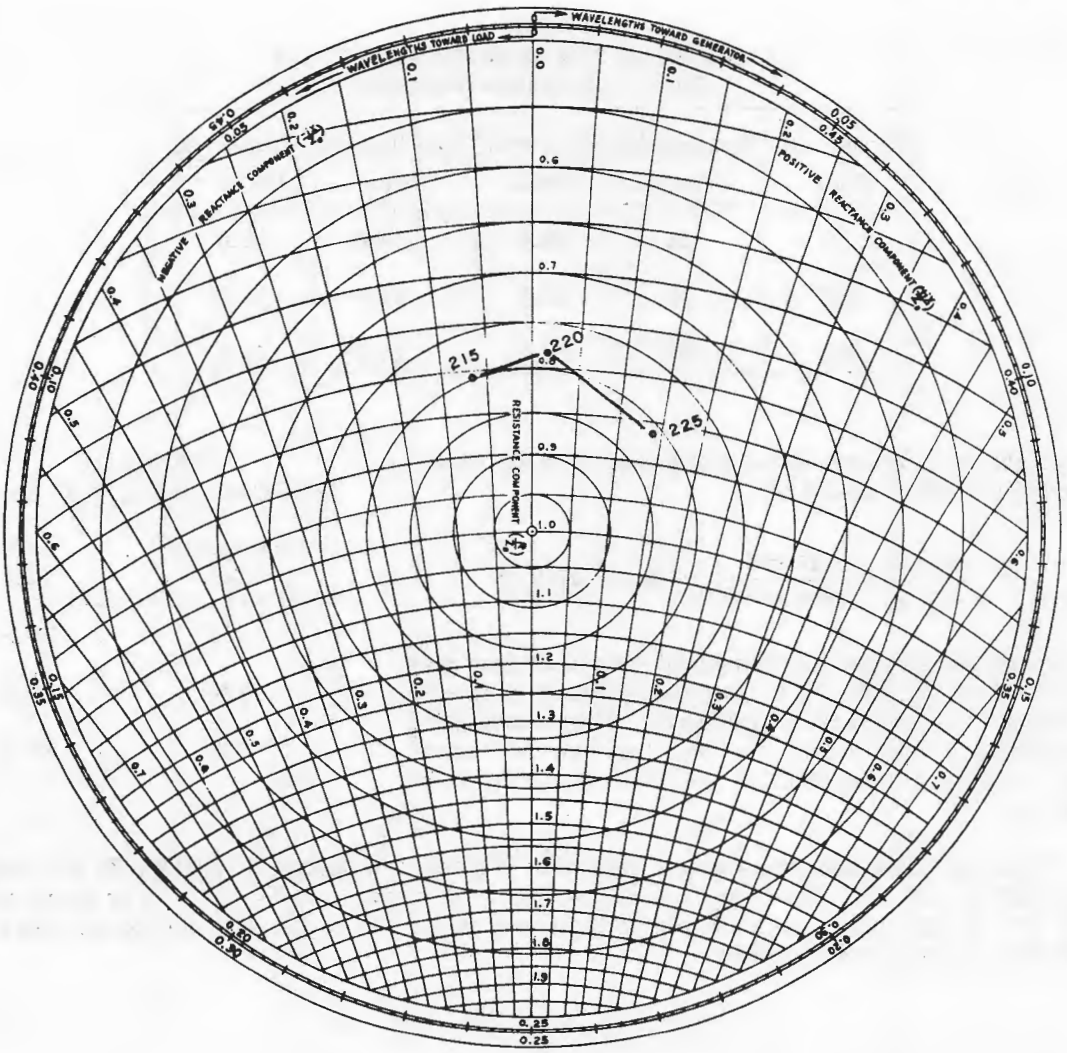

Fig. 37 - Input impedance of the 33-1/2-foot antenna

The power breakdown in the antenna was observed with the transmitter delivering 900 watts average power and the pressure in the coaxial line reduced to simulate flying the antenna at high altitudes. When the pressure was reduced to correspond to conditions at 15,000 feet, no breakdown was observed in the rotary joint or feed line. At 17,000 feet some arcing occurred in the coaxial line. Since the operating altitude of the ZPG-2W airship is 4000 feet, it is considered that there is no danger of power breakdown.

[redacted]

PART IV - THE HEIGHT FINDER

A. G. Ferris

When a meter-wave radar is operated at high altitudes, as in an airplane or airship, the sea-reflection interference pattern provides a possible method of height-finding on isolated aircraft targets. One method is based on searchlighting the target with the radar and counting the number of lobes traversed as it approaches or recedes. An evaluation of this height-finding method at 220 Mc is one of the goals of this airborne-radar program.

There are a number of limitations on this technique as a height-finding method. However, the simplicity and small size of the equipment, and the range to which adequate height information can be obtained (dependent on the radar range) may make this technique valuable until a more sophisticated approach now being pursued can yield results. This latter approach employs frequency-modulation techniques and will ease the restrictions on height-finding methods utilizing the interference pattern (16).

This lobe-counting investigation in conjunction with the work at 425 Mc (7,8) will give information on the stability of the interference pattern, the influence of sea clutter, and other data which will be useful in this new approach.

THEORY

The sea-reflection interference pattern is the result of the vector addition of energy reaching the target via two paths. The path difference between the direct and reflected paths is

$$\Delta R = \frac{2h_r\, h_t}{r}\, J(S,T)$$

where

h_r is the radar height

h_t is the target height

r is the target range

$J(S,T)$ is a correction factor from a flat to a spherical earth (9)

S is a function of h_r, h_t, and r

T is a function of h_r and h_t.

When the range of the target changes sufficiently to alter the path difference by one wavelength, the target passes from one lobe to the next. Therefore, the number of lobes L traversed per nautical mile is

[redacted]

$$L = \frac{1}{\lambda}\left|\frac{d(\Delta R)}{dr}\right| = \frac{2h_r\, h_t}{\lambda}\left|\left[-\frac{J}{r^2} + \frac{1}{r}\,\frac{dJ}{dr}\right]\right|.$$

Theoretical curves can be derived from this equation relating lobes per nautical mile, range, target altitude, and radar altitude for a given radar frequency. The use of these curves in determining altitude is complicated and difficult because of the nonlinear character of the relationship and the necessity of interpolating between curves to obtain target height. A calculator, or slide rule, incorporating all parameters has been developed and a model for a frequency of 425 Mc is shown in Fig. 38. A similar rule is being made for 220 Mc.

DESCRIPTION

Height-finding by the lobe-counting method requires isolation of a target from all others in both range and azimuth. The instrumentation discussed here includes a range-gated tracker which, together with the horizontal directivity, isolates the target echo, and the equipment which records the variations of echo amplitude with range.

A block diagram of the primary units of the system is shown in Fig. 39. A 10-nautical-mile interval of range is selected from the 250-nautical-mile radar presentation and is displayed on a 3-inch A-scope. At the center of this interval a 2-μsec segment is selected. This bit of range is shown as a negative marker on the scope, and a gate of the same width is used to gate an i-f amplifier. The rejection ratio in the gated i-f amplifier is 40 to 50 db. The gated signal is amplified, demodulated using a peak detector and a thyratron to hold the peak voltage until just prior to the next sample, and applied to one channel of a standard Brush model BL-262 recorder. Range information to the nearest nautical mile is available from the position of the i-f gate, and is displayed on a Veeder-Root counter. In addition, 5-nautical-mile range marks are generated for the first 200 nautical miles and processed with the i-f gate to give a mark on the second channel of the recorder every 5 nautical miles (i.e., at 5, 10, 15, 20 nautical miles, etc.) as the target opens or closes. Photographs of the tracker and recorder are shown in Figs. 40 and 41.

The equipment described here will be operated from a single station. The necessary recorder controls are remoted to the tracker. Rate-aided tracking has been added to assist the operator. After the initiation of a track a few adjustments of the speed-control rheostat should be sufficient to maintain range track with a minimum of correction. Experience has shown that a second operator stationed at a PPI display with antenna hand slew can maintain the target in the antenna beam satisfactorily. These operators, although tracking the same target in different coordinates, function independently.

RESULTS AND CONCLUSIONS

There has been no preliminary height-finding data obtained on the 220-Mc system. Expected operating conditions have been simulated in the Laboratory and the tracker and recorder have been calibrated and checked. No difficulty is anticipated in operating them with the radar in the airship.

The program for the investigation of height-finding by the lobe-counting method will be similar to that at 425 Mc (7,8), but of wider scope. At 425 Mc it was possible to use

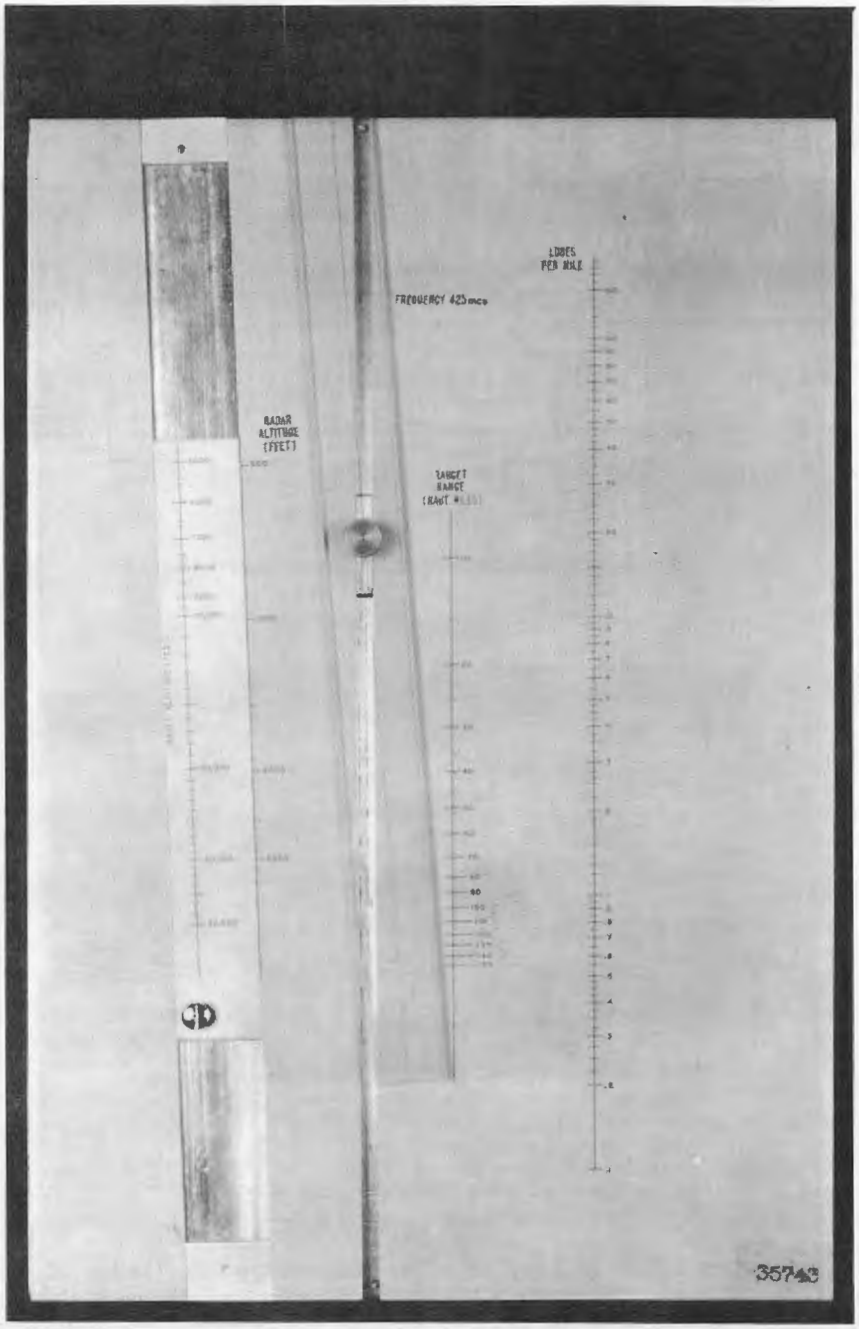

Fig. 38 - Lobe-counting slide rule

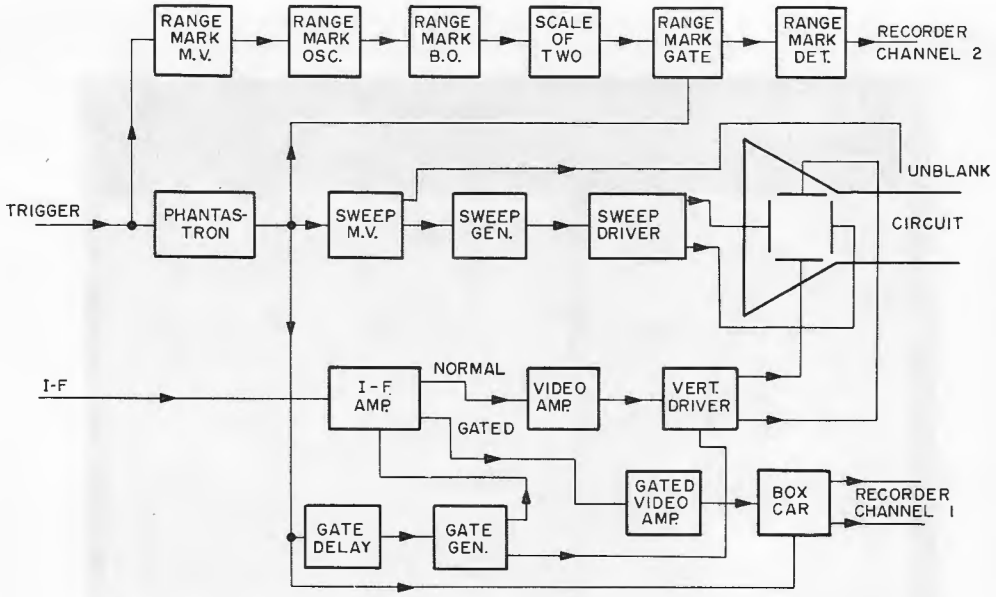

Fig. 39 - Block diagram of the range-gated tracker

Fig. 40 - Tracker unit

this method to determine height of a target of the bomber type to a range of about 100 nautical miles (approximately 90 percent of detection range) at all sea states through and including sea state 5. Because of the greater system sensitivity of the 220-Mc system and the greater coarseness of the lobe structure at that frequency, it is expected that the useful range of height-finding will be approximately 150 nautical miles or 75 percent of the detection range for a similar target. Rough seas should not be a problem insofar as their effect on height-finding is concerned.

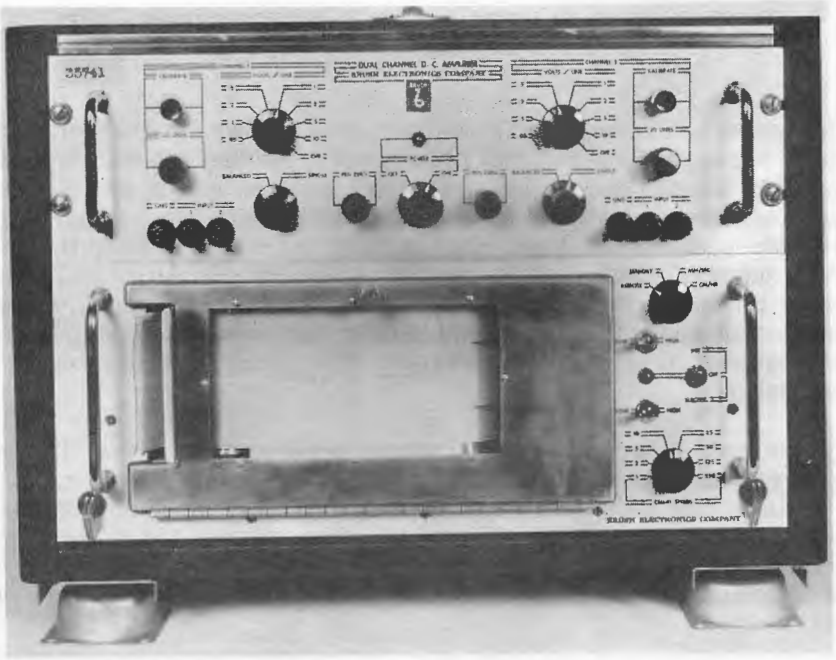

Fig. 41 - Recorder unit

FUTURE PLANS

The lobe-counting instrumentation discussed here, like that used at 425 Mc, is essentially a research tool. It is designed for use where a number of controlled range tracks of 100 to 250 nautical miles are to be made and the data processed in identical range increments for all tracks. To utilize this technique operationally a relatively short (approximately 10 nautical miles) single range increment will be used. Consequently a substantial reduction in the size, weight, and complexity will be realized by eliminating certain features such as the automatic range markers and rate-aided tracking, by changing from i-f gating to video gating, and by simplification of the recorder. The Bureau of Aeronautics is negotiating with the Goodyear Aircraft Corporation to incorporate a limited-duty height-finder of this type in the newer and larger ZPG-3W airship. A description and discussion of the proposed system is included in the final report on the lobe-counting trials at 425 Mc (8).

In addition to the lobe-counting trials at 220 Mc an investigation will be made of possible ways of further improving the utility of the height finder from an operational standpoint. A two-phase program will be followed. The goal of the first phase is the elimination of the recorder by shaping the lobing signal and counting the lobes electronically with sufficient accuracy. The successful completion of this task will lead directly into phase two, the development and testing of circuitry for indicating the range of the sample and computing the rate of lobe crossing, L'. The ultimate objective is to read out target height quickly, easily, and automatically on a counter or dial using the range and lobes-per-mile circuitry developed in this program.

PART V - THE CLUTTER-GATED NONCOHERENT MTI

G. W. Hermann

The clutter-gated noncoherent MTI has been chosen over the coherent type for use in the airship radar because of the difficult problem of achieving satisfactory velocity compensation. Investigation of the requirements which must be met in order to compensate an MTI system for movement of an airborne vehicle shows that the radial velocity to be compensated is dependent on the depression angle of the clutter. Since this angle varies with range, the amount of compensation must vary with range. Although the exact required amount of compensation can be described mathematically for all ranges, no practical means of applying such compensation to a coherent system has been developed. A noncoherent system, which requires no velocity compensation has therefore been chosen for the airborne MTI application.

Normally, the main disadvantage of the noncoherent system is that it cannot distinquish moving targets in the absence of clutter. The clutter gate however, automatically switches the system from MTI operation to normal operation when no clutter is present. This switching from one mode of operation to the other enables the radar to present a composite picture of moving targets over the whole area scanned by the radar. Figure 42 shows a block diagram of the complete system. Photographs of the unit are shown in Figs 43 and 44.

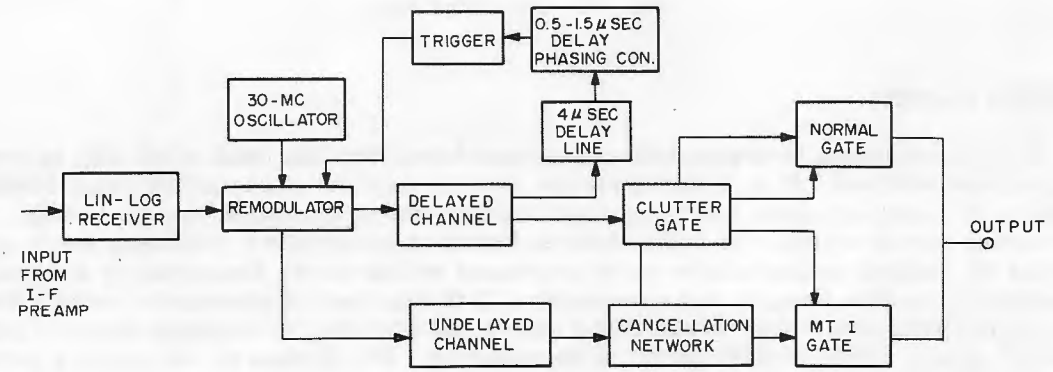

Fig. 42 - MTI system block diagram

The present system uses two fused-quartz delay lines to obtain the necessary 3300-μsec delay. Two lines are used because of the impracticability of getting one line of such long delay in a small enough package.

The MTI works on the principle that the phase of a moving target varies from sweep to sweep, while the phase of a stationary target does not. The returning echo from clutter is used as a reference against which the moving target returns are compared. The varying phase of the moving target is translated into an amplitude variation in the receiver detector. The detected target return is used to modulate a 30-Mc oscillator and is then fed to both a delayed carrier channel and an undelayed carrier channel. The gains of these two channels must be as nearly equal as possible, to ensure that maximum cancellation

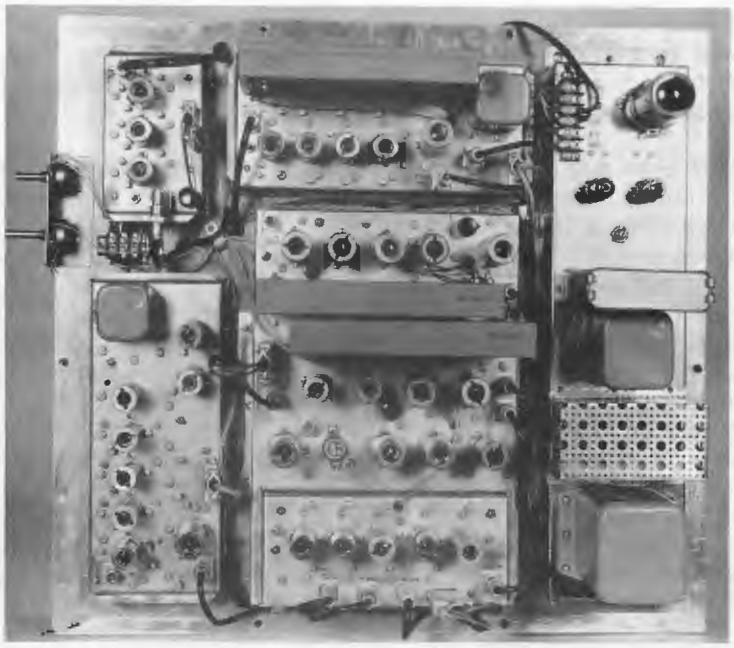

Fig. 43 - Top view of the MTI unit

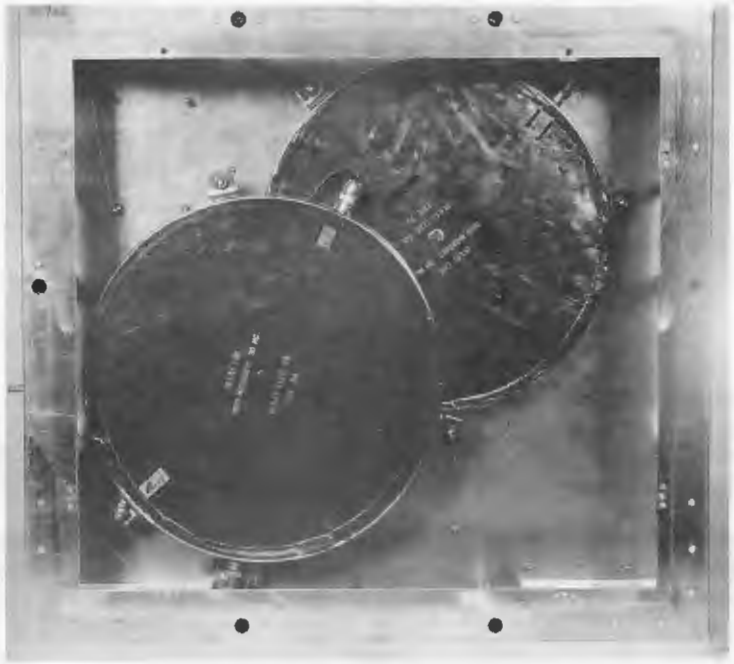

Fig. 44 - Bottom view of the MTI unit

will take place. For this reason there is a manual gain control in the undelayed carrier amplifier which may be adjusted to equalize the gain through the two channels. If the gains are not equal, a difference voltage will be obtained from the cancellation network, which will appear falsely as a moving target.

The clutter gate uses pulse-width discrimination to distinquish between clutter areas and areas free of clutter. Consider a target of 5-μsec pulse width appearing in the system. (Five μsec is the duration of the transmitter pulse and represents the pulse width of an echo from an isolated target.) The pulse is fed to one grid of a twin-triode gate generator (12AT7, Fig. 45). At the same time this pulse is fed through a 5-μsec delay line, where a delayed normal video is extracted to be supplied to the normal gate. The delayed pulse is fed through a second 5-μsec delay line and to the other grid of the gate generator. By means of plate mixing a split gate will be formed. This gate consists of two intervals, each of 5-μsec duration, with one preceding and one following the delayed normal signal. This gate wave is applied to both the MTI (gate on) and normal (gate off) gate tubes. In the case cited, the 5-μsec echo will occur between the two intervals of the gate wave, and will thus be passed by the normal channel. On the other hand, a longer echo received by the system will be assumed to be clutter; it will cause the two intervals of the gate wave to merge, forming a single gate beginning 5 μsec before the start of the clutter and persisting until 5 μsec after the end of the echo. Thus, the system will be switched to MTI 5 μsec before the start of the clutter and returned to normal 5 μsec after the clutter ends.

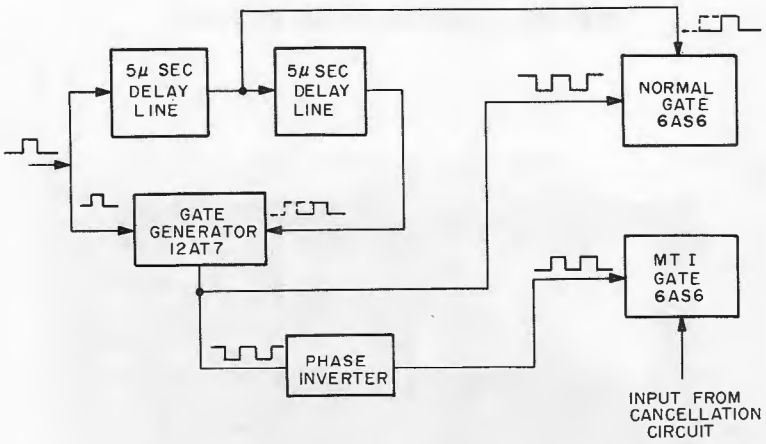

Fig. 45 - Clutter gate block diagram

If a moving target appears in the clutter, there will be an output from the cancellation circuit, and since the MTI gate is conducting, the target will pass through the gate. Plate mixing of the normal and MTI gates is used to obtain the composite picture of moving targets whether in clutter or not.

The completed MTI system is expected to have a video cancellation ratio of about 30 db. System instabilities, scanning losses, etc., are expected to degrade subclutter-visibility of the complete MTI radar to about 24 db.

* * *

ACKNOWLEDGMENTS

Although only a few of the individuals of the Search Radar Branch are named in this report, the various radar components are the collective work of many members of the Branch.

Goodyear Aircraft Corporation personnel have contributed freely to the solution of technical problems involved in the unique installation of this equipment in the airship. Their cooperation has also been appreciated.

* * *

REFERENCES

1. BuAer Ltr AER-EL-4315 ser 020322 (~~Confidential~~) to Dir NRL, dtd 19 October 1954

2. Main, W. F., and Alderson, W. S., "A Low-Frequency Radar of Modern Design," NRL Report 3815 (~~Confidential~~), May 1951

3. Blake, L. V., Carlson, D. J., Herring, R. A., Jr., "A Study of 220- and 425-Megacycle Shipboard Radar for Long-Range Detection," NRL Report 4840 (~~Confidential~~), November 1956

4. Alderson, W. S., Blake, L. V., Guthrie, R. C., "A Preliminary Consideration of Meter-Wave Airborne Barrier Radar," enclosure to letter C-3930-139/53ijk of 25 June 1953 (~~Confidential~~)

5. Franta, A. L., Herring, R. A., Jr., and Shoemaker, J. R., "An Experimental UHF Radar for AEW," NRL Report 4504 (~~Confidential~~), March 1955

6. Blake, L. V., "A Proposed Method of Height-Finding with VHF and UHF Airborne Radar," NRL Report 4549 (~~Confidential~~), June 1955

7. Ferris, A. G., and Franta, A. L., "Height-Finding with UHF AEW Radar," Report of NRL Progress (~~Confidential~~), July 1955

8. Ferris, A. G., and Franta, A. L., "Height-Finding by the Lobe-Counting Method," NRL Report (in preparation).

9. Kerr, D. E., "Propagation of Short Radio Waves," New York:McGraw-Hill, Radiation Laboratory Series, Vol. 13, 1951, pp. 113-122

10. MacDonald, F. C., NRL Ltr to Chief of Naval Operations, C-5270-77/54

11. MacDonald, F. C., NRL Ltr to Chief of Naval Operations, C-5270-1/55

12. Blake, L. V., "Comparison of Predicted and Experimental Ranges of Some Developmental Navy Search Radars," NRL Memorandum Report 611 (~~Confidential~~), June 1956

13. "Handbook Service Instructions, Radar Set AN/APS-20B, AN-16-30APS20-32" (~~Confidential~~), published under authority of the Secretary of the Air Force and the Chief of the Bureau of Aeronautics, 15 June 1953

14. "Supplement to Handbook Service Instructions, Radar Set AN/APS-20B" (~~Confidential~~), 15 June 1954

15. Hoffman, Lawrence, "A Low Noise 215-225 Mc Converter," NRL Report 4765, June 1956

16. Chambers, T. H., "A Frequency-Modulated Height-Finding Radar Operating on the Interference Principle," NRL Report 4738 (~~Confidential~~ report, Unclassified title), 30 April 1956

17. Marcuvitz, N., "Waveguide Handbook," New York:McGraw-Hill, Radiation Laboratory Series, Vol. 10, 1951, p. 353 and p. 370

18. Shoemaker, J. R., and Randall, C. R., "220- and 435-Mc Antenna for the AN/SPS-17 Radar," NRL Report 4323 (~~Confidential~~), April 1954

19. Carter, P. S., "Circuit Relations in Radiating Systems and Applications to Antenna Problems," Proc. I.R.E., 20:1004, June 1932

20. Cork, E. C., et al., "Feeder and the Like for Electrical Currents of High Frequency," U. S. Patent 2,138,906

21. Riblet, H. J., "Slotted Dipole Impedance Theory," M.I.T. Radiation Laboratory Report 772, 21 November 1945

* * *

[redacted] NAVY-DPPO PRNC. WASH., D.C.